

Parameterization of basal hydrology near grounding lines

G. R. Leguy et al.

This discussion paper is/has been under review for the journal The Cryosphere (TC).
Please refer to the corresponding final paper in TC if available.

Parameterization of basal hydrology near grounding lines in a one-dimensional ice sheet model

G. R. Leguy^{1,2}, X. S. Asay-Davis^{2,3,4}, and W. H. Lipscomb²

¹New Mexico Institute of Mining and Technology, 801 Leroy Place, Socorro, New Mexico 87501, USA

²Los Alamos National Laboratory, Los Alamos, New Mexico 87545, USA

³Courant Institute of Mathematical Sciences, New York University, 251 Mercer Street, New York, New York 10012-1185, USA

⁴Potsdam Institute for Climate Impact Research, Telegraphenberg A 31, 14473 Potsdam, Germany

Received: 4 December 2013 – Accepted: 9 December 2013 – Published: 14 January 2014

Correspondence to: G. R. Leguy (gunter@nmt.edu)

Published by Copernicus Publications on behalf of the European Geosciences Union.

Title Page

Abstract

Introduction

Conclusions

References

Tables

Figures

⏪

⏩

◀

▶

Back

Close

Full Screen / Esc

Printer-friendly Version

Interactive Discussion



Abstract

Ice sheets and ice shelves are linked by the transition zone, the region where the grounded ice lifts off the bedrock and begins to float. Adequate resolution of the transition zone is necessary for numerically accurate ice sheet–ice shelf simulations. The required resolution depends on how the basal physics is parameterized. We propose a new, simple parameterization of the basal hydrology in a one-dimensional vertically integrated model. This parameterization accounts for connectivity between the basal hydrological system and the ocean in the transition zone. Our model produces a smooth transition between finite basal friction in the ice sheet and zero basal friction in the ice shelf. Through a set of experiments based on the Marine Ice Sheet Model Intercomparison Project (MISMIP), we show that a smoother basal shear stress, in addition to adding physical realism, significantly improves the numerical accuracy of our fixed-grid model, allowing for reliable grounding-line dynamics at resolutions ~ 1 km.

1 Introduction

Antarctica's contribution to sea level rise has increased in the past decade. While the contribution of the East Antarctic Ice Sheet (EAIS) remains steady, mass loss from the West Antarctic Ice Sheet (WAIS) has more than doubled (Velicogna, 2009; Rignot et al., 2011). Theoretical models suggest that marine ice sheets like WAIS are susceptible to instabilities when they lie on bedrock that slopes upward in the direction of ice flow (Weertman, 1974; Schoof, 2007a). If these instabilities are triggered, mass loss will accelerate, exacerbating future sea-level rise and potentially leading to WAIS collapse (Vaughan and Spouge, 2002; Joughin and Alley, 2011). For this reason it is important to understand the dynamic processes that drive ice sheets in the region.

The glaciology community has developed many ice-sheet models of varying complexity. Full–Stokes models (Durand et al., 2009; Favier et al., 2012) are considered to be the gold standard because they include all components of the stress tensor. How-

TCD

8, 363–419, 2014

Parameterization of basal hydrology near grounding lines

G. R. Leguy et al.

Title Page

Abstract

Introduction

Conclusions

References

Tables

Figures

◀

▶

◀

▶

Back

Close

Full Screen / Esc

Printer-friendly Version

Interactive Discussion



Parameterization of basal hydrology near grounding lines

G. R. Leguy et al.

Title Page

Abstract

Introduction

Conclusions

References

Tables

Figures

◀

▶

◀

▶

Back

Close

Full Screen / Esc

Printer-friendly Version

Interactive Discussion



ever, they are not widely used at continental scales due to their large computational cost, especially in three dimensions. By neglecting terms in the stress tensor, modelers have derived and applied several simpler, computationally cheaper approximations to the Stokes equations, including the first-order model (Pattyn, 2003; Perego et al., 2012), the so-called L1L2 model (Hindmarsh, 2004; Schoof and Hindmarsh, 2010; Cornford et al., 2013), the shallow-ice approximation (Rutt et al., 2009; Bueler and Brown, 2009), and the shallow-shelf approximation (MacAyeal, 1989; Schoof, 2007a). Many models, regardless of their complexity, require very fine resolution (< 1 km) in the transition zone (the region where the grounded ice lifts off the bedrock and begins to float) in order to obtain numerically accurate ice sheet–ice shelf simulations (Durand et al., 2009; Cornford et al., 2013). Pattyn et al. (2006) and Gladstone et al. (2010a) showed that higher-order interpolation at the grounding line, the transition point between the grounded ice sheet and floating ice shelf, could vastly reduce the error in the grounding-line position, implying convergence at coarser resolution. The physically based parameterization introduced in this paper typically results in further reduction of this error, with the added advantage that the width of the resulting transition zone is essentially independent of model resolution.

Several studies have investigated the effects of different friction laws on ice dynamics using one-dimensional, depth-integrated models (Muszynski and Birchfield, 1987; MacAyeal, 1989; Schoof, 2007a). Vieli and Payne (2005) and Schoof (2007a) prescribed a discontinuous friction law across the grounding line where the ice loses contact with the bed. In these models the friction is nonzero in the ice sheet, but abruptly falls to zero at the grounding line. Both models have the drawback that the accuracy of the grounding-line dynamics strongly depends on grid resolution. A tolerance of a few kilometers in the grounding-line location requires a resolution on the order of tens to hundreds of meters (Durand et al., 2009; Gladstone et al., 2010a, b; Cornford et al., 2013), which is computationally prohibitive for large-scale simulations. This requirement was confirmed by the Marine Ice Sheet Model Intercomparison Project (MISMIP, Pattyn et al., 2012) which used the same basal friction law as in Schoof (2007a). In

this project, participants using a variety of fixed-grid models found that the errors in grounding-line position were unacceptably high (100 km or more) at resolutions that were computationally feasible in three-dimensional models (~ 1 km).

One way to reduce the computational cost is to use adaptive mesh refinement (Goldberg et al., 2009; Gladstone et al., 2010b; Cornford et al., 2013), i.e., to subdivide the horizontal mesh near features where high resolution is needed. Durand et al. (2009) investigated this approach in a full-Stokes model with the basal friction law of Schoof (2007a). They performed a set of experiments described in the MISMIP project with the goal of reaching neutral equilibrium in grounding line position when using very high resolution near the grounding line. Even with grid resolution of 30 m in the transition zone, they found differences in the grounding-line position over an advance-and-retreat cycle of ~ 2 km, whereas theoretical arguments predict that there should be no difference.

In order to reduce the need for high resolution near the grounding line, Pattyn et al. (2006) proposed a smooth basal-friction parameter that decays exponentially to zero as the ice flows across the grounding line into the ice shelf. This approach gave promising results, as the transition zone could be partially resolved even at 12.5 km grid resolution, but the model introduced an arbitrary length scale of exponential decay, and the basal friction remained nonzero (though small) in the ice shelf.

Martin et al. (2011) used a friction law that depends on basal water pressure, prescribed to be 96 % of overburden pressure under the marine portion of the Antarctic Ice Sheet, including close to the grounding lines. This parameterization reduced, but did not fully eliminate the discontinuity in basal friction at the grounding line. Furthermore, they concluded that the 20 km resolution used in their model was too coarse to properly resolve the ice-sheet margins.

In the case of rapidly sliding ice streams, basal resistance is controlled by the underlying water-laden plastic till (Tulaczyk et al., 2000a, b; van der Wel et al., 2013). The presence of liquid water lowers the effective pressure at the ice base, leading to reduced basal friction (Tulaczyk et al., 2000b; Carter and Fricker, 2012; van der Wel et al., 2013), an effect not accounted for in many ice sheet models. Recent ob-

Parameterization of basal hydrology near grounding lines

G. R. Leguy et al.

Title Page

Abstract

Introduction

Conclusions

References

Tables

Figures



Back

Close

Full Screen / Esc

Printer-friendly Version

Interactive Discussion



Parameterization of basal hydrology near grounding lines

G. R. Leguy et al.

Title Page

Abstract

Introduction

Conclusions

References

Tables

Figures

◀

▶

◀

▶

Back

Close

Full Screen / Esc

Printer-friendly Version

Interactive Discussion



servations confirm the existence of basal drainage channels that connect subglacial lake systems (Wingham et al., 2006; Fricker et al., 2009). Episodic drainage events lead to regions of decreased basal friction and rapid sliding of overlying ice streams. Some of these drainage systems are found near grounding lines (Fricker and Scambos, 2009; Carter and Fricker, 2012), meaning that they are likely to connect to the ocean (Le Brocq et al., 2013). Another type of basal water channel forms through pressure-induced melt. Channels of this type that form within 50 to 100 km of the grounding line are also likely to connect to the ocean (Cuffey and Paterson, 2010). Tidal uplift causes horizontal migration of grounding lines (Holland, 2008; Makinson et al., 2012), suggesting strong hydrological connectivity between the ice base and the ocean within a few kilometers of the grounding line.

In this paper, we propose a new parameterization of basal hydrology near the grounding line that we combine with an established friction law linking basal stress and sliding to the local water pressure. This representation provides a physically motivated, smooth transition between finite basal friction in the ice sheet and zero basal friction in the ice shelf.

Previous models have included the effect of basal water pressure or meltwater thickness in their friction laws (Bueler and Brown, 2009; Pimentel et al., 2010; Martin et al., 2011). Some models (Budd et al., 1979; Budd and Jenssen, 1989) have included the effect of hydrological connectivity between basal channels and the ocean. These models were motivated by laboratory experiments, which supported the idea that a friction law should include the effective pressure, the difference between the ice overburden pressure and the water pressure at the bed. Though Schoof (2005) later showed that the friction law in Budd et al. (1979) and Budd and Jenssen (1989) was unphysical, their work inspired our own study.

In Sect. 2 we present our one-dimensional, vertically integrated flowline model, including a new parameterization of basal hydrology and its relationship to the basal friction law. Based on this parameterization we give a new definition of the transition zone. We also discuss mathematical limits of the basal friction law and the numerical

methods used for our simulations. In Sect. 3 we show simulation results with different hydrological connectivity parameter values for different bedrock topographies. In Sect. 4 we discuss these results, the limitations of our model, and the implications for future development of three-dimensional ice-sheet models. A more detailed description of the numerical method is provided in Appendix A.

2 Model

The shallow-shelf flowline model presented in this paper, which is similar to the model of Schoof (2007a), is one-dimensional, symmetric and depth-integrated. It includes the effect of three stress terms: the longitudinal stress (τ_l), the basal stress (τ_b), and the driving stress (τ_d). The model neglects lateral shear (and therefore buttressing) and vertical shear, and thus is best used to simulate fast-flowing ice streams. While additional physics would be required to model realistic ice sheets, our model provides a simple, computationally efficient tool for idealized studies of grounding-line dynamics.

2.1 Model equations

The model consists of an equation for the evolution of ice thickness (conservation of mass) and a vertically integrated stress-balance equation:

$$H_t + (uH)_x = a, \quad (1)$$

$$\tau_l + \tau_b + \tau_d = 0, \quad (2)$$

where subscripts x and t denote partial derivatives (e.g. $H_t \equiv \frac{\partial H}{\partial t}$). The ice thickness H , ice velocity u , and other important model variables are defined in Table 1. Table 2 gives the value of the accumulation rate a and other model parameters. The one-dimensional model is intended to represent the motion of a transversely and vertically averaged ice stream. Derivations of Eqs. (1) and (2) can be found in Muszynski and Birchfield (1987)

Parameterization of basal hydrology near grounding lines

G. R. Leguy et al.

Title Page

Abstract

Introduction

Conclusions

References

Tables

Figures

◀

▶

◀

▶

Back

Close

Full Screen / Esc

Printer-friendly Version

Interactive Discussion



and MacAyeal (1989). From Schoof (2007a), the longitudinal- and driving-stress terms are

$$\tau_l = \left[2\bar{A}^{-\frac{1}{n}} H |u_x|^{\frac{1}{n}-1} u_x \right]_x, \quad (3)$$

$$\tau_d = -\rho_i g H s_x. \quad (4)$$

The first term, τ_l , is the vertically integrated viscous stress with nonlinear viscosity given by Glen's flow law, where \bar{A} is the depth-averaged ice softness and n is the Glen's flow exponent. The second term, τ_d , is the gravitational stress that drives ice flow in the direction of decreasing surface elevation, where ρ_i , g and s_x are ice density, gravitational acceleration and ice surface slope, respectively.

Equations (1)–(4) apply to both the ice sheet and the ice shelf. The surface elevation s is computed differently in the two regions – from the bedrock elevation and ice thickness in the ice sheet, and from exact flotation in the ice shelf:

$$s = \begin{cases} H - b & x < x_g \\ \left(1 - \frac{\rho_i}{\rho_w}\right) H & x \geq x_g \end{cases}, \quad (5)$$

where b is the bedrock elevation. We adopt the convention of Schoof (2007a) that b is positive below sea level.

Basal stress beneath ice shelves is zero everywhere. Under the ice sheet, the basal-friction law takes the form given in Schoof (2005):

$$\tau_b = -C |u|^{\frac{1}{n}-1} u \left(\frac{N^n}{\frac{m_{\max}}{\lambda_{\max} A_b} |u| + N^n} \right)^{\frac{1}{n}}, \quad (6)$$

where C is the constant shear stress factor defined in Schoof (2007a), the effective pressure $N \equiv \rho_i - \rho_w$ is the difference between the overburden pressure $p_i \equiv \rho_i g H$ and the basal water pressure p_w , A_b is the ice softness at the bed chosen based on an ice

Parameterization of basal hydrology near grounding lines

G. R. Leguy et al.

Title Page

Abstract

Introduction

Conclusions

References

Tables

Figures

◀

▶

◀

▶

Back

Close

Full Screen / Esc

Printer-friendly Version

Interactive Discussion



Parameterization of basal hydrology near grounding lines

G. R. Leguy et al.

Title Page

Abstract

Introduction

Conclusions

References

Tables

Figures

◀

▶

◀

▶

Back

Close

Full Screen / Esc

Printer-friendly Version

Interactive Discussion



temperature of -2°C , and λ_{\max} and m_{\max} are the wavelength of bedrock bumps and the maximum bed obstacle slope, respectively. These last two parameters represent bedrock roughness at scales too small to be resolved in the model. As we will discuss further in Sect. 2.2, Eq. (6) was proposed in Schoof (2005) as an ad hoc non-linear extension of the linear friction law ($n = 1$) with the appropriate behavior in the limits of both slower-flowing, thicker ice in the ice-sheet interior and more rapidly sliding, thinner ice near grounding lines. Gagliardini et al. (2007) numerically validated this ad hoc formulation as a limiting case of their own friction law. We have modified the notation from Schoof (2005) to match that of Schoof (2007a) in the limit of slow flow and large effective pressure.

We assume the ice sheet to be symmetric at the ice divide, the origin of the domain, leading to the following boundary conditions:

$$u = 0 \quad \text{at} \quad x = 0, \quad (7)$$

$$(H - b)_x = 0 \quad \text{at} \quad x = 0, \quad (8)$$

At the grounding line, the requirement of exact flotation leads to the boundary condition

$$H = \frac{\rho_w}{\rho_i} b \quad \text{at} \quad x = x_g. \quad (9)$$

Combining Eqs. (2)–(5), the stress balance in the ice shelf is given by

$$\left[2\bar{A}^{-\frac{1}{n}} H |u_x|^{\frac{1}{n}-1} u_x \right]_x - \rho_i \left(1 - \frac{\rho_i}{\rho_w} \right) g H H_x = 0. \quad (10)$$

At the calving front the ice shelf is subject to the ocean backpressure, $p_w = -\rho_w g z$, between the ice shelf base, $z = (\rho_i / \rho_w) H$, and sea level, $z = 0$. The ocean pressure partially (but not completely) balances the hydrostatic pressure of the ice,

$\rho_i = -\rho_i g(z - s)$. The force on the ice shelf due to the difference in hydrostatic pressure between the ice shelf and the ocean is:

$$f_p(x_c) = \int_{-(\rho_i/\rho_w)H}^s -\rho_i g(z - s) dz - \int_{-(\rho_i/\rho_w)H}^0 -\rho_w g z dz$$

$$= \frac{1}{2} \rho_i \left(1 - \frac{\rho_i}{\rho_w} \right) g H^2. \quad (11)$$

The force on the calving face due to longitudinal (viscous) stress must compensate for this imbalance in hydrostatic pressure:

$$2\bar{A}^{-\frac{1}{n}} H |u_x|^{\frac{1}{n}-1} u_x = \frac{1}{2} \rho_i \left(1 - \frac{\rho_i}{\rho_w} \right) g H^2 \quad \text{at } x = x_c. \quad (12)$$

Following Schoof (2007a), we integrate Eq. (10) from the calving front ($x = x_c$) to the grounding line ($x = x_g$), and use Eq. (12) to show that the same condition holds at the grounding line as at the calving front:

$$2\bar{A}^{-\frac{1}{n}} H |u_x|^{\frac{1}{n}-1} u_x = \frac{1}{2} \rho_i \left(1 - \frac{\rho_i}{\rho_w} \right) g H^2 \quad \text{at } x = x_g. \quad (13)$$

In order for the stresses to remain finite, H , u and u_x must be continuous across the grounding line.

2.2 Basal hydrology and friction law

Most models of marine ice sheets assume that the basal friction jumps discontinuously to zero across the grounding line. In reality, this transition must occur over a finite length scale. We propose a mechanism for this smooth transition. We adopt the friction law from Schoof (2005), validated and extended in Gagliardini et al. (2007). This

Title Page

Abstract

Introduction

Conclusions

References

Tables

Figures

◀

▶

◀

▶

Back

Close

Full Screen / Esc

Printer-friendly Version

Interactive Discussion



Parameterization of basal hydrology near grounding lines

G. R. Leguy et al.

Title Page

Abstract

Introduction

Conclusions

References

Tables

Figures

◀

▶

◀

▶

Back

Close

Full Screen / Esc

Printer-friendly Version

Interactive Discussion



formulation, given by Eq. (6), has the correct limits for large values of the effective basal pressure, and reduces to Coulomb friction in the limit of small effective pressure. Schoof (2005) suggested that this friction law was an appropriate simplification for rough terrain; Gagliardini et al. (2007) showed that this limiting case of their more general friction law (corresponding to their decay parameter $q = 1$) was appropriate for sawtooth terrain. They also argued that this limit of their friction law may lead to better behavior in numerical models because the relation between basal stress and sliding velocity is monotonic.

If the water pressure is continuous across the grounding line, the basal shear stress falls to zero at the grounding line, allowing a smooth transition between grounded and floating ice. Assuming that the subglacial drainage system is connected to the ocean, the water pressure at the ice-sheet base will be close to the ocean pressure at that depth, reaching the ocean pressure at the grounding line (with pressure differences driving flow through the drainage system). A simple function for the effective pressure that accounts for ocean water pressure is

$$N(p) = \rho_i g H \left(1 - \frac{H_f}{H} \right)^p, \quad (14)$$

in which we introduce a parameter p that varies between zero (no basal water pressure) and one (the subglacial drainage system is hydrologically well connected to the ocean). The effective basal pressure $N(p)$ has the following desired limits:

- When $p = 0$, $N(p) = \rho_i g H$ (no water-pressure support).
- When $p = 1$, $N(p) = \rho_i g (H - H_f)$ (full water-pressure support from the ocean wherever the ice-sheet base is below sea level).
- At the grounding line when $p > 0$, $N(p) = 0$ (τ_b is continuous across the grounding line).

The flotation thickness is defined by $H_f \equiv \max\left(0, \frac{\rho_w}{\rho_i} b\right)$. Note that $H_f = 0$ and $N = \rho_i g H$ when the bedrock is above sea level ($b < 0$). When $H_f/H \ll 1$ and the bedrock is below

Parameterization of basal hydrology near grounding lines

G. R. Leguy et al.

Title Page

Abstract

Introduction

Conclusions

References

Tables

Figures

◀

▶

◀

▶

Back

Close

Full Screen / Esc

Printer-friendly Version

Interactive Discussion



sea level ($b > 0$), the fraction of the bed with water-pressure support approaches ρ . In general, because H rises steeply inland of the grounding line, $H_f/H \ll 1$ for much of the grounded portion of the ice sheet. Therefore, the hydrological-connectivity parameter ρ can be said to define the fraction of the hydrological system on the inland side of the transition zone that has connectivity to the ocean.

Figures 1 and 2 show typical ice-sheet geometry, thickness, H_f/H and N for five values of ρ over linear and polynomial bedrock topography, respectively. In both cases, the smaller the ρ value the bigger the effective pressure, which tends to move the grounding line seaward. The jump in effective pressure is to be expected for $\rho = 0$ because of the limit defined above. This jump remains for small values of ρ because the transition zone is not big enough to be resolved in our model. The figures show that the effective pressure drops to zero with increasing smoothness as ρ increases, meaning that the basal stress will also be increasingly smooth.

In our one-dimensional model, values of $0 \leq \rho \leq 1$ in Eq. (14) represent the fraction of the basal area over which water at ocean pressure is able to provide basal lubrication, averaged over the width of the channel. Our model represents only the portion of water-pressure support related to the ocean; basal water pressure in the model falls to zero when the bedrock reaches sea level ($b = 0$). More sophisticated models of basal till find that the basal water pressure remains a significant fraction of the overburden pressure in much of the ice-sheet interior (Tulaczyk et al., 2000b; van der Wel et al., 2013). A more complex model might include a network of channels as well as water-laden till at the base of ice streams. This hydrological network would influence the basal friction through water-pressure support outside the transition zone.

Parameterized in terms of ρ , Eq. (6) becomes

$$\tau_b = -C|u|^{\frac{1}{n}-1} u \left(\frac{N(\rho)^n}{\kappa|u| + N(\rho)^n} \right)^{\frac{1}{n}}, \quad (15)$$

where $\kappa \equiv \frac{m_{\max}}{\lambda_{\max} A_b}$. This formulation does not require the introduction of an arbitrary length scale of basal transition, as in the parameterization proposed by Pattyn et al.

(2006). Equation (15) has two asymptotic behaviors. Within the bulk of the ice sheet, the ice is thick and slow moving, so that $\kappa u \ll N(\rho)^n$ and

$$\tau_b \approx -C|u|^{\frac{1}{n}-1}u. \quad (16)$$

Note that in this limit, τ_b is independent of ρ . Many ice-sheet models define the basal friction law throughout the ice sheet to have the form of Eq. (16), as is the case in both Schoof (2007a) and the MISMIP experiments. This simplified friction law leads to a set of equations with an accurate semi-analytic approximation (Schoof, 2007a), whereas the more complex friction law in Eq. (15) does not, to the best of our knowledge, lend itself to a similar semi-analytic solution. Nevertheless, the semi-analytic solution of Schoof (2007a) closely approximates our model as ρ approaches zero. Figure 3a shows that the basal-stress term (blue) closely matches the limit of high overburden pressure (red) given by Eq. (16) when $\rho = 0$. In this limit, the boundary-layer solution and our high-resolution benchmark solution differ by a few kilometers or less.

The second asymptote, the Coulomb-friction limit, occurs near the grounding line where the ice is thin and fast-flowing, so that $\kappa u \gg N(\rho)^n$ and

$$\tau_b \approx -\frac{C}{\kappa^{\frac{1}{n}}}N(\rho)^{\frac{1}{n}}\frac{u}{|u|}. \quad (17)$$

By construction, when $\rho = 0$ the effective pressure is equal to the full overburden pressure, p_i , and the basal stress discontinuously drops to zero across the grounding line. When $\rho > 0$, the effective pressure N smoothly approaches zero at the grounding line over a distance that increases as ρ increases.

In the transition zone just inland of the grounding line, the basal stress is proportional to the effective pressure. We define this transition zone by those locations in the ice sheet where $0 \leq N(\rho)^n \leq \kappa u$. We find that the transition zone covers a distance between 0 and ~ 20 km, depending on ρ , the bedrock topography, and the ice softness. Importantly, the size of the transition zone is an increasing function of ρ , meaning that, at a given resolution, the transition zone is better resolved when ρ is larger. Figure 3b

Parameterization of basal hydrology near grounding lines

G. R. Leguy et al.

Title Page

Abstract Introduction

Conclusions References

Tables Figures

◀ ▶

◀ ▶

Back Close

Full Screen / Esc

Printer-friendly Version

Interactive Discussion



Discussion Paper | Discussion Paper | Discussion Paper | Discussion Paper | Discussion Paper

line, we compute the basal and driving stresses once each assuming that the cell is entirely grounded and then entirely floating. Finally, the stresses are linearly interpolated between their grounded and floating values, based on the fraction of the cell that is grounded vs. floating. The resulting expressions of the basal and driving stresses are given by Eqs. (A38) and (A39), respectively. We chose not to use the quadrature methods employed in Gladstone et al. (2010a) because they would likely be too cumbersome and costly in 3-D ice-sheet models. In simulations without a GLP, the model computes basal and driving stresses as if the cell containing the grounding line were entirely grounded.

We discretize the equations of motion on a staggered grid, shown in Fig. 4, with alternating velocity and thickness points (u - and H -points). The ice divide ($x = 0$) and the calving front are placed at a u -point and an H -point, respectively, allowing us to satisfy both boundary conditions naturally. We included a ghost H -point to the left of the ice divide to ensure zero surface slope at the divide. The details of the numerics for the fixed-grid model are given in Appendix A1, and a full description of the GLP is given in Appendix A2.

To evaluate the performance of the fixed-grid model, we needed a benchmark solution to compare with our fixed-grid results. To this end we implemented a stretched-grid, pseudo-spectral method using Chebyshev polynomials (Boyd, 2001) to produce spectrally accurate steady-state benchmark results. The Chebyshev collocation points are non-uniformly distributed over the ice-sheet domain, with the highest resolution at the grounding line and ice divide. Using 1025 Chebyshev modes, the grid spacing continuously decreases from ~ 80 m at a distance of 2 km from the grounding line, to ~ 2.5 m at the grounding line. The Chebyshev code produces grounding-line positions that match the semi-analytic solution of Schoof (2007a) to within millimeters (when the appropriate terms are neglected) and converges to error tolerances of less than one part in 10^{10} , giving us confidence in the accuracy of the benchmark results. The full details of the method are given in Appendix A3.

Parameterization of basal hydrology near grounding lines

G. R. Leguy et al.

[Title Page](#)[Abstract](#)[Introduction](#)[Conclusions](#)[References](#)[Tables](#)[Figures](#)[◀](#)[▶](#)[◀](#)[▶](#)[Back](#)[Close](#)[Full Screen / Esc](#)[Printer-friendly Version](#)[Interactive Discussion](#)

3 Results

The results described in this section are based on the MISMIP experiments (Pattyn et al., 2012). These experiments are designed to study the transient behavior of marine ice-sheet models. For a given ice softness A we obtain a steady ice-sheet profile.

This profile is then used as the initial condition for the next experiment, which evolves to a new steady state with a new value of the ice softness. MISMIP experiment 1 prescribes decreasing values of A and linear bedrock topography, leading to an advancing grounding line. MISMIP experiment 2 is experiment 1 in reverse, where A is increased back to its original value, resulting in grounding-line retreat. Experiment 3 is similar to the combination of experiments 1 and 2, but using a polynomial bedrock topography. The values of A for experiments 1 and 2 are given in Table 3, while those for experiment 3 are given in Table 4. A full description of the MISMIP experiments can be found at <http://homepages.ulb.ac.be/~fpattyn/mismip/>.

Models participating in the MISMIP intercomparison used the friction law of Schoof (2007a), which is equivalent to Eq. (16). For our experiments we test two model configurations, *non-GLP* and *GLP*, both of which include the friction law from (15), with effective pressure defined by Eq. (14). The *GLP* configuration includes the grounding-line parameterization discussed in Sect. 2.3 and Appendix A2, while the *non-GLP* configuration does not. We tested five values of the hydrological-connectivity parameter ρ equally spaced between zero and one. Note that only our results when $\rho = 0$ can be directly compared with the results of Pattyn et al. (2012). By changing the value of ρ , we are changing the physics, not just the numerics, of the problem. Aside from the modified friction law and associated parameterization of basal hydrology, we used the standard MISMIP protocols except as specifically stated below.

3.1 Estimating errors

In general, we compute errors in our fixed-grid result by comparing them to Chebyshev benchmark solutions. In order to give us confidence that the benchmark solutions are

TCD

8, 363–419, 2014

Parameterization of basal hydrology near grounding lines

G. R. Leguy et al.

Title Page

Abstract

Introduction

Conclusions

References

Tables

Figures

◀

▶

◀

▶

Back

Close

Full Screen / Esc

Printer-friendly Version

Interactive Discussion



accurate, we compared the Chebyshev results with the semi-analytic boundary-layer model from Schoof (2007a) known as *Model A*. The boundary-layer model was derived by neglecting longitudinal stresses except in a boundary layer near the grounding line, using the friction law from Eq. (16), and applying boundary conditions given by Eqs. (9) and (13).

We configured our benchmark code with the same simplifying assumptions, and found that we were able to reproduce grounding-line positions from *Model A* to within fractions of a millimeter (the error tolerance of the Chebyshev solver). When we include the full longitudinal stress in the Chebyshev model, we found that differences with the *Model A* grounding-line position increased to ~ 1 km. Switching to the more complex basal friction law, Eqs. (14) and (15), introduced further differences of order 1 km or less. We attribute the differences between *Model A* and the Chebyshev solution with full longitudinal stress and our friction law to the simplifying assumptions of *Model A*, rather than to errors in the Chebyshev model. These results give us confidence that the Chebyshev model is producing solutions with errors that should be negligible (of order meters or less) compared to those from the fixed-grid model (order kilometers or more). In the remainder of the text, we will refer to *estimated error* in a quantity as the absolute value of the difference in that quantity between the fixed-grid and benchmark Chebyshev solution at a given value of A .

Typically, differences in grounding-line positions are used to compare the accuracy of ice-sheet model results (Pattyn et al., 2012). This measure is practical for us as well, since the grounding-line position is easily diagnosed from both Chebyshev and fixed-grid simulations. In realistic simulations, errors in grounding-line position are not as important as those in volume above flotation, which is directly related to the ice sheet's contribution to sea-level change. However, we found (not shown) that the behavior of both metrics is qualitatively similar: large (small) errors in grounding-line position correspond to large (small) errors in volume above flotation.

In addition to computing the maximum error over an advance-and-retreat cycle, we introduce another metric of error, *FMI* ("Final Minus Initial"), referring to the difference

Parameterization of basal hydrology near grounding lines

G. R. Leguy et al.

[Title Page](#)[Abstract](#)[Introduction](#)[Conclusions](#)[References](#)[Tables](#)[Figures](#)[◀](#)[▶](#)[◀](#)[▶](#)[Back](#)[Close](#)[Full Screen / Esc](#)[Printer-friendly Version](#)[Interactive Discussion](#)

between the final grounding-line position after an advance-and-retreat cycle and the initial position. *FMI* is designed to measure the ability of the model to return to its initial state, as in Durand et al. (2009), and is similar to the *RMA* (“Retreat Minus Advance”) metric used by Gladstone et al. (2010a). Experiments with large *FMI* errors show numerical hysteresis in the fixed-grid solution that is absent in the semi-analytic and benchmark solutions.

3.2 Linear-bed experiments

We performed a series of experiments with the linear bedrock topography of Schoof (2007a), shown in Fig. 1a:

$$b(x) = - \left(720 - 778.5 \frac{x}{750 \text{ km}} \right) \text{ m.} \quad (18)$$

We forced the ice sheet first to advance and then to retreat by varying the ice softness A , in analogy to MISMIP experiments 1 and 2 (Pattyn et al., 2012). To force ice-sheet advance, we incrementally decreased A through the values listed in Table 3, allowing the ice sheet to evolve to steady state each time A is changed. Then, to force retreat, we increased A through the same values in reverse order, again evolving to steady state at each step. Experiments were performed at three resolutions (3.2, 1.6 and 0.8 km), five values of p (0, 0.25, 0.5, 0.75 and 1), and both with and without the GLP.

Schoof (2007a, b) showed that the steady-state grounding-line position on a bed sloping monotonically downward in the direction of the ice flow is unique for a given ice softness. Figure 5 shows the grounding-line positions derived from the boundary-layer solution of Schoof (2007a) and those from advance-and-retreat cycles using our Chebyshev and fixed-grid models with $p = 0$ at 0.8 km resolution. The grounding-line position in our Chebyshev simulation differs from that of the boundary-layer solution by less than 1.2 km. As mentioned in the previous section, this difference appears to be mostly due to the fact that the boundary-layer model neglects longitudinal stresses in the bulk of the ice sheet.

Parameterization of basal hydrology near grounding lines

G. R. Leguy et al.

Title Page

Abstract

Introduction

Conclusions

References

Tables

Figures

⏪

⏩

◀

▶

Back

Close

Full Screen / Esc

Printer-friendly Version

Interactive Discussion



The grounding-line position in the fixed-grid model advances relatively accurately, whether or not the GLP is applied, with errors of no more than 22 km. The benefit of the GLP becomes clear during the retreat phase of the experiment: the fixed-grid model overestimates the grounding-line position by as much as 220 km when the GLP is not used, but by no more than 28 km with the GLP included.

Figure 6 shows the differences between the grounding-line position from the fixed-grid and benchmark models in several configurations: both without (left) and with (right) GLP, and at three different resolutions, 3.2 km (top), 1.6 km (middle) and 0.8 km (bottom). We show differences, rather than estimated errors (the absolute value of the differences), because the sign of the difference is important in telling whether the grounding line is too far advanced or too far retreated. During the retreat phase of each experiment (the right-hand side of each plot), the fixed-grid grounding line is always too advanced, whereas during the advance phase (the left-hand side of each plot), the grounding line may be too advanced or too retreated depending on the values of ρ and the ice softness A . For simulations with $\rho < 0.5$ with and without the GLP, the grounding-line position is not sufficiently advanced during the advance phase. For simulations with $\rho > 0.5$, the grounding-line position is always too advanced during the full experiment.

The same behavior can be seen more quantitatively in Table 5, which gives two error metrics for the simulation results at all three resolutions. The *max err* is the maximum value of the estimated error over both advance and retreat phases, given in km. The *FMI* is the difference between the grounding-line position at the end of the advance-and-retreat cycle, and the initial value given in km. These two metrics are also given as a percentage of the total change in grounding-line position over the retreat phase measured by the benchmark code. We used the absolute value of both metrics to express them as percentages.

Both the figure and the table show that the estimated errors decrease approximately linearly with the grid-cell size for each value of ρ , either with or without the GLP. Linear convergence of grounding-line errors with resolution has been seen in other fixed-grid

Parameterization of basal hydrology near grounding lines

G. R. Leguy et al.

Title Page

Abstract

Introduction

Conclusions

References

Tables

Figures

◀

▶

◀

▶

Back

Close

Full Screen / Esc

Printer-friendly Version

Interactive Discussion



models (Gladstone et al., 2010a; Cornford et al., 2013). Compared with resolution, the application of the GLP and the increase of the hydrological-connectivity parameter p from zero to one produce a much more dramatic reduction in estimated error. The improvement is particularly apparent during the retreat phase of each experiment (right-hand side of Fig. 6). The experiments most similar to typical MISIP fixed-grid results – experiments without GLP and with $p = 0$ (red dots in the left-hand column) – show huge estimated errors during retreat on the order of hundreds of kilometers. The estimated errors decrease by approximately a factor of ten in both the experiments with a GLP at $p = 0$ (red dots in the right-hand column) and the experiments *without* a GLP but with $p = 1$ (blue dots in the left-hand column). Surprisingly, the combination of the GLP and the hydrology parameterization with $p = 1$ (blue dots in the right-hand column) does not seem to have particular advantages over $p = 1$ but without the GLP, showing diminished performance particularly during retreat. In the next subsection, we will show that the same is not true for polynomial bedrock topography.

The GLP has essentially no impact on the advance phase (left-hand side of Fig. 6), whereas the behavior during advance does tend to improve as p increases. This improvement can be seen in two ways. First, the estimated error is less volatile as a function of A . Second, whether or not the GLP is present, the model is increasingly good at returning to its original grounding-line position at the end of the advance-and-retreat cycle as p increases (the *FMI* metric in Table 5). Without a GLP, the *FMI* values are on the order of hundreds of kilometers when $p = 0$, but less than 14 km at 3.2 km resolution, 3 km at 1.6 km resolution and 0.01 km at 0.8 km resolution when $p = 1$.

Assuming a maximum error in grounding-line position of $\sim 5\%$ to be acceptable, Table 5 shows that there is a trade-off between resolution and smoothness of the basal stress, as determined by p or the GLP. With the GLP and a resolution of 1.6 km or finer, nearly any value of p will produce an acceptable error. Errors at 3.2 km are somewhat larger than the threshold regardless of p . Without the GLP, only the largest values of p produce acceptable errors. At 0.8 km resolution, the experiment with $p = 0.75$ also meets the criterion.

hysteresis behavior within the range of A prescribed by MISMIP experiment 3. For a given ice softness, lower basal friction (i.e., larger ρ) tends to move the grounding line inland, as shown in Fig, 2, so that the grounding line never reaches the unstable region for larger values of ρ . In order to obtain hysteresis, we added five smaller values of A to the experiments with $\rho = 0.75$ and $\rho = 1$. These additional values are included in the rightmost column of Table 4.

When $\rho = 0$, the boundary-layer solution of Schoof (2007a) model A again provides a good approximation of our equations of motion. Figure 7 shows the grounding-line positions derived from the boundary-layer solution together with the positions from experiments using our Chebyshev and fixed-grid models with $\rho = 0$. The grounding line of the boundary-layer solution differs from that in our Chebyshev benchmark simulations by less than 1.4 km, similar to the linear bed experiments. The fixed-grid model at 0.8 km resolution performs well during the advance phase both with and without the GLP; the grounding line is always in the same region (either 1 or 3) as the benchmark solution. The maximum error is about 34 km without the GLP and about 15 km with the GLP. However, without the GLP, the model performs poorly during the retreat phase, where the grounding line never retreats across the unstable region leading to an error of about 700 km. Such an error is unacceptably large when trying to forecast sea level rise. Furthermore, the error in the fixed-grid solution is as high as 110 km even when the fixed-grid and benchmark grounding lines are in the same region. In contrast, the fixed-grid model with the GLP follows the Chebyshev solution more accurately, with a maximum error of ~ 35 km when the grounding line computed by both models lies in the same region. In this case the fixed-grid model succeeds in re-crossing the unstable region.

Pattyn et al. (2012) showed that fixed-grid models often have trouble re-crossing the unstable region during the retreat phase. We found this to be true only for small values of ρ without a GLP, where the transition zone is poorly resolved. Figure 8 shows fixed-grid grounding-line position minus that of the benchmark solution at three resolutions (3.2 km in the top row, 1.6 km in the middle row and 0.8 km in the bottom row) both

Parameterization of basal hydrology near grounding lines

G. R. Leguy et al.

[Title Page](#)[Abstract](#)[Introduction](#)[Conclusions](#)[References](#)[Tables](#)[Figures](#)[⏪](#)[⏩](#)[◀](#)[▶](#)[Back](#)[Close](#)[Full Screen / Esc](#)[Printer-friendly Version](#)[Interactive Discussion](#)

Parameterization of basal hydrology near grounding lines

G. R. Leguy et al.

Title Page

Abstract

Introduction

Conclusions

References

Tables

Figures

◀

▶

◀

▶

Back

Close

Full Screen / Esc

Printer-friendly Version

Interactive Discussion



large errors in grounding-line position near the critical value of A . For values of $\rho < 1$, the largest errors occur further away from the unstable region, suggesting that these errors instead result from the increasing difficulty that the fixed-grid model has with re-treating as ρ decreases. Overall, these results suggest that the fixed-grid model can capture hysteresis with increasing fidelity as ρ increases and (to a lesser extent) as resolution increases, and that errors nearly always decrease at a given value of x_g as ρ increases.

Figure 9 also suggests that errors may be a strong function of bedrock slope. The largest errors occur near the local maximum in bed elevation at around $x = 1.25 \times 10^3$ km, and decrease sharply as the bedrock steepens further into region 3. Similar inverse correlation between bed slope and error can be seen in region 1, though the steepening is less dramatic in this region. Based on this behavior, we surmise that what appeared to be a systematic bias in many of the linear-bed experiments is, in fact, a slope dependent error which cannot be corrected by model tuning.

As in the previous section, we examine the maximum error in grounding-line position of the fixed-grid results (*max error*) as well as the measure of error in the transient response of the model over the full advance-and-retreat cycle (*FMI*). These errors are shown for all three resolutions in Table 6. The change in grounding-line position over the retreat phase is not the strongly decreasing function of ρ in these experiments that it was with the linear bed topography. Unlike in the linear-bed experiments, including the GLP does not significantly reduce the error for the smallest values of ρ .

Again, we will assume that errors in grounding-line position of $\sim 5\%$ of the total change in grounding-line position over the retreat phase are tolerable. Inclusion of the GLP slightly increases the range of ρ values that produces acceptable errors. When the GLP is included, only those experiments at 0.8 km resolution with $\rho \geq 0.25$ or at 1.6 km resolution with $\rho \geq 0.75$ meet the criterion. At 3.2 km, results fall just outside this threshold even with $\rho = 1$.

The *FMI* metric shows that whenever the grounding line successfully retreats to region 1, the model is able to return to its initial state at the end of the advance-and-retreat

Parameterization of basal hydrology near grounding lines

G. R. Leguy et al.

Title Page

Abstract

Introduction

Conclusions

References

Tables

Figures

⏪

⏩

◀

▶

Back

Close

Full Screen / Esc

Printer-friendly Version

Interactive Discussion



cycle with a high degree of accuracy. The *FMI* error is less prone to being dominated by outliers than the *max err* (e.g., in the experiment with $p = 1$ at 1.6 km resolution without the GLP). Since the benchmark solution (as well as theoretical arguments) puts the initial and final state of each experiment in a region with a unique grounding-line position, the *FMI* error shows the increasing ability of the model to return to the initial, unique solution as p increases and/or with the addition of the GLP.

The polynomial bed in these experiments represents a more realistic topography than the linear bed. Local maxima and minima, absent in the linear topography, have a significant impact on both model dynamics and numerical errors. Our experiments suggest that, depending on the value of p , it may be possible to produce grounding-line dynamics with errors of tens of kilometers, as opposed to hundreds of kilometers, with a fixed-grid model at 1 km resolution or coarser. This is achieved either by using large values of p , the GLP, or both.

4 Conclusions

Using the MISMIP benchmark experiments, we have shown several advantages of a novel, physically based basal-hydrology parameterization together with an appropriate basal-friction law. The new parameterization accounts for hydrological connectivity between basal melt water and the ocean, allowing basal friction to decrease smoothly to zero at the grounding line. Our results suggest that grounding-line dynamics in a fixed-grid model with smoother basal stress (corresponding to larger values of the hydrological-connectivity parameter p) converge to a given error tolerance with much coarser resolution than does a model with discontinuous basal sliding ($p = 0$).

Errors in the grounding-line position are typically reduced as hydrological connectivity to the ocean increases and basal stress becomes smoother even when a numerical grounding-line parameterization (GLP) is also used; the two techniques appear to be complementary.

Previous research has suggested that grounding-line position converges with increasing resolution (Vieli and Payne, 2005), typically linearly (Gladstone et al., 2010a; Cornford et al., 2013). We find this to be true in our simulation. However we do not observe the numerical instability seen at coarser resolution in Gladstone et al. (2010a) or the premature retreat found in the fixed-grid model of Goldberg et al. (2009), as seen in their Fig. 4b. Instead, with the use of our basal-hydrology parameterization and assuming good connectivity to the ocean ($p \sim 1$), we find that a fixed-grid approach at relatively coarse resolution shows promising results.

Assuming these results extend to three-dimensional models, the implications are significant. The grounding-line position converges at ~ 1 km grid resolution or coarser when the lubricating effects of sub-glacial hydrology near the grounding line are included, whereas much finer resolution of $\lesssim 200$ m is needed when the friction law is discontinuous at the grounding line (Cornford et al., 2013). This implies that it may be possible to simulate marine ice sheets at much lower computational expense than would be required with traditional friction laws. Our parameterization could allow uniform-grid models to simulate whole ice sheets, since ~ 1 km resolution throughout the ice sheet is feasible though expensive. Also, models with adaptive and unstructured grids (Goldberg et al., 2009; Favier et al., 2012; Perego et al., 2012; Cornford et al., 2013) could be made more computationally cost effective by decreasing the finest resolution to ~ 1 km. Importantly, the combination of both our basal parameterization with $p \sim 1$ and a GLP may reduce errors sufficiently to allow for useful fixed-grid simulations at ~ 3 km resolution or coarser.

Our basal-hydrology parameterization is designed to ensure a smooth transition between a dry bed and a frictionless ice-shelf base at flotation. The parameterization is by no means a sophisticated till model. Rather, it focuses on the part of the hydrological system that is connected to the ocean and reaches ocean pressure at the grounding line. The parameter p in our model affects basal sliding only near the grounding line (within 20 km in our experiments), where ocean water pressure is a significant fraction of overburden pressure. This is consistent with Cuffey and Paterson (2010), who sug-

Parameterization of basal hydrology near grounding lines

G. R. Leguy et al.

[Title Page](#)[Abstract](#)[Introduction](#)[Conclusions](#)[References](#)[Tables](#)[Figures](#)[◀](#)[▶](#)[◀](#)[▶](#)[Back](#)[Close](#)[Full Screen / Esc](#)[Printer-friendly Version](#)[Interactive Discussion](#)

continuous (or nearly continuous) across the grounding-line. However, in the absence of a basal-friction law, such as ours, that is affected by changes in the grounding-line location, as time evolves the grounding line will advance or retreat but C will remain fixed in space. This is likely to lead to large jumps in basal stress across the grounding line at later times, and to non-convergent grounding-line dynamics at coarser resolution. A primary advantage of our parameterization is that, for larger values of ρ , the basal stress remains continuous and smooth over a resolvable transition zone even as the grounding line migrates.

In the near future we plan to incorporate our parameterization into the Community Ice Sheet Model (CISM), a three-dimensional model with support for a variety of higher-order stress approximations, several types of grids, and coupling to global climate models (Rutt et al., 2009; Perego et al., 2012; Lipscomb et al., 2013). We envision inverting for the parameter ρ near the grounding line in similar fashion to how spatially varying values of C are typically derived. Along flowlines in regions where $\kappa u \geq N(\rho)^n$ (the region over which ρ has an impact on the solution), we would hold C fixed at its nearest upstream value and invert for the value of $0 \leq \rho \leq 1$ that best matches present-day velocity, thickness, thickness change and accumulation rate. This approach, however, would not eliminate the need for very high resolution in regions where ρ is close to zero. For a fixed-resolution model, this would defeat the purpose of the parameterization. To counter this problem, a simple GLP could be used. Also, we could invert for ρ once using present-day data and obtain a map of ρ values. From this map, we could derive average values of ρ for large regions or for the entire Antarctic ice sheet. Doing so would increase the model accuracy in some regions. In other regions basal stresses might be less accurate, but the parameterization could act as a regularization term. In any case, physical and numerical parameterizations would reduce the need for very high resolution near the grounding line.

Parameterization of basal hydrology near grounding lines

G. R. Leguy et al.

[Title Page](#)[Abstract](#)[Introduction](#)[Conclusions](#)[References](#)[Tables](#)[Figures](#)[⏪](#)[⏩](#)[◀](#)[▶](#)[Back](#)[Close](#)[Full Screen / Esc](#)[Printer-friendly Version](#)[Interactive Discussion](#)

Appendix A

Numerics

Here we describe the numerical methods behind the fixed-grid, finite-difference model and the stretched-grid Chebyshev model. We hope this will facilitate comparison with other modeling algorithms. In what follows, we denote vectors with bold italics and matrices with bold capital letters.

A1 Fixed-grid model without a GLP

In the fixed-grid model, we used staggered finite difference to solve Eqs. (1)–(4), (7)–(9), (13) and (15), rewritten here for convenience:

$$H_t + (uH)_x = a, \quad (\text{A1})$$

$$2A^{-\frac{1}{n}}(H|u_x|^{\frac{1}{n}-1}u_x)_x - C|u|^{\frac{1}{n}-1}u\left(\frac{N(\rho)^n}{\kappa|u| + N(\rho)^n}\right)^{\frac{1}{n}} - \rho_i gH(H-b)_x = 0, \quad (\text{A2})$$

$$u = 0 \quad \text{at } x = 0, \quad (\text{A3})$$

$$(H-b)_x = 0 \quad \text{at } x = 0, \quad (\text{A4})$$

$$H = \frac{\rho_w}{\rho_i}b \quad \text{at } x = x_g. \quad (\text{A5})$$

$$2A^{-\frac{1}{n}}|u_x|^{\frac{1}{n}-1}u_x - \frac{1}{2}\rho_i\left(1 - \frac{\rho_i}{\rho_w}\right)gH = 0 \quad \text{at } x \geq x_g. \quad (\text{A6})$$

We use centered differences to discretize Eqs. (A2)–(A6) on a uniform grid. To insure numerical stability, we use a first-order upwinding scheme and a semi-implicit time stepping scheme to discretize Eq. (A1).

We compute u and H on staggered grids separated by half a grid cell, as shown on Fig. 4. The ice-sheet-ice-shelf domain contains $N + M$ points, where N is the number

TCO

8, 363–419, 2014

Parameterization of basal hydrology near grounding lines

G. R. Leguy et al.

Title Page

Abstract

Introduction

Conclusions

References

Tables

Figures

◀

▶

◀

▶

Back

Close

Full Screen / Esc

Printer-friendly Version

Interactive Discussion



of points in the ice sheet (changing in time as the grounding line migrates) and M the number of points in the ice shelf on both the H -grid.

Since the boundary conditions in Eq. (A3) and (A4) are most easily satisfied at a u -grid point, we place the ice divide, $x = x_d = 0$, at the first point on the u -grid. In general, the grounding-line position, $x = x_g$, lies between two grid points and is diagnosed from H using Eq. (A5), the flotation condition. The boundary condition given by Eq. (A6) applies in the entire ice shelf domain.

We found that it simplified computations near the ice divide to place a “ghost” H -grid point to the left of the divide; we enforce symmetry by requiring that the ice thickness is symmetric across the ice divide, that is $H_1 = H_2$, satisfying Eq. (A4). Similarly, we find that a ghost point beyond the calving-front, this time on the u -grid, makes it easier to simultaneously solve Eq. (A2) at the last “real” u -grid point and Eq. (A6) at the calving front. This ghost point is also needed to solve Eq. (A1) at the calving front.

Excluding the two half-cells associated with these ghost points, there are $2(N + M) - 3$ half-cells between the ice divide and the calving front on the staggered grid. Thus, the spacing between points on both the H - and u -grids is given by

$$\Delta x = \frac{L}{N + M - \frac{3}{2}}, \quad (\text{A7})$$

where $L = x_c - x_d$ denotes the length of the domain.

For an integer index $i \in [1, N + M]$, we define the location of H -grid points by $x_i \equiv (i - 3/2)\Delta x$ and those of u -grid points by $x_{i+1/2} \equiv (i - 1)\Delta x$. Similarly, we introduce a time index $j \in [1, T]$, where T is the number of time steps in a given simulation, so that $t_j = j\Delta t$ for a constant time step Δt .

Discrete values of thickness and velocity, are $H_i^j \equiv H(x_i, t_j)$ and $u_{i+1/2}^j \equiv u(x_{i+1/2}, t_j)$, respectively. The grounding line position is defined as $x_g^j = x_g(j\Delta t)$. The depth of the ice-sheet bed is defined as $b_i \equiv b(x_i)$ at H -points and by $b_g = b(x_g)$ at the grounding line. The effective pressure, $N(x, t; p)$, is located on an H -grid point and is defined by

Parameterization of basal hydrology near grounding lines

G. R. Leguy et al.

Title Page

Abstract

Introduction

Conclusions

References

Tables

Figures



Back

Close

Full Screen / Esc

Printer-friendly Version

Interactive Discussion



$\mathcal{N}_i^j \equiv N(x_i, t_j; \rho)$ (not to be confused with the number of ice-sheet grid points N):

$$\mathcal{N}_i^j = \rho_i g H_i^j \left(1 - \frac{H_{f_i}}{H_i^j} \right)^p. \quad (\text{A8})$$

The flotation thickness, H_f , is defined at H -grid points as

$$H_{f_i} \equiv H_f(x_i) = \max(0, b_i \rho_w / \rho_i). \quad (\text{A9})$$

Equation (A1) is discretized at H -grid points throughout the domain (both ice sheet and ice shelf):

$$\frac{H_i^{j+1} - H_i^j}{\Delta t} + \theta \mathcal{F}_i^{j+1} + (1 - \theta) \mathcal{F}_i^j = a, \quad (\text{A10})$$

where

$$\mathcal{F}_i^j \equiv \frac{\left(H_{\text{up}, i+\frac{1}{2}}^j u_{i+\frac{1}{2}}^j - H_{\text{up}, i-\frac{1}{2}}^j u_{i-\frac{1}{2}}^j \right)}{\Delta x}, \quad (\text{A11})$$

and where we have used first-order upwinding, with the upwind thickness defined by

$$H_{\text{up}, i+\frac{1}{2}}^j = \begin{cases} H_i^j & \text{if } u_{i+\frac{1}{2}}^j \geq 0, \\ H_{i+1}^j & \text{if } u_{i+\frac{1}{2}}^j \leq 0. \end{cases} \quad (\text{A12})$$

The time centering is determined by $0 \leq \theta \leq 1$: If $\theta = 1$, the time stepping is fully implicit; if $\theta = 0$, we are using a fully explicit scheme; and if $\theta = 1/2$, the method is the partially implicit, second-order accurate in time Crank–Nicholson scheme.

Equation (A2) is most naturally discretized at u -grid points, requiring that the thickness, H , in the driving stress and the effective pressure, \mathcal{N} , in the friction law be averaged to the u -grid, e.g. $H_{i+\frac{1}{2}}^j = (H_i^j + H_{i+1}^j)/2$. In the grounded ice sheet, Eq. (A2) in discrete form is

$$\begin{aligned}
 & \frac{2A^{-\frac{1}{n}}}{\Delta x^{1+\frac{1}{n}}} \left[H_{i+1}^j \left| u_{i+\frac{3}{2}}^j - u_{i+\frac{1}{2}}^j \right|^{\frac{1}{n}-1} \left(u_{i+\frac{3}{2}}^j - u_{i+\frac{1}{2}}^j \right) - H_i^j \left| u_{i+\frac{1}{2}}^j - u_{i-\frac{1}{2}}^j \right|^{\frac{1}{n}-1} \left(u_{i+\frac{1}{2}}^j - u_{i-\frac{1}{2}}^j \right) \right] \\
 & - C \left| u_{i+\frac{1}{2}}^j \right|^{\frac{1}{n}-1} u_{i+\frac{1}{2}}^j \left[\frac{\left(\frac{\mathcal{N}_{i+1}^j + \mathcal{N}_i^j}{2} \right)^n}{\kappa |u_{i+\frac{1}{2}}^j| + \left(\frac{\mathcal{N}_{i+1}^j + \mathcal{N}_i^j}{2} \right)^n} \right]^{\frac{1}{n}} \\
 & - \rho_i g \frac{(H_{i+1}^j + H_i^j)}{2} \frac{(H_{i+1}^j - b_{i+1} - H_i^j + b_i)}{\Delta x} = 0.
 \end{aligned} \tag{A13}$$

In the ice shelf, Eq. (A2) is discretized as

$$\begin{aligned}
 & \frac{2A^{-\frac{1}{n}}}{\Delta x^{1+\frac{1}{n}}} \left[H_{i+1}^j \left| u_{i+\frac{3}{2}}^j - u_{i+\frac{1}{2}}^j \right|^{\frac{1}{n}-1} \left(u_{i+\frac{3}{2}}^j - u_{i+\frac{1}{2}}^j \right) - H_i^j \left| u_{i+\frac{1}{2}}^j - u_{i-\frac{1}{2}}^j \right|^{\frac{1}{n}-1} \left(u_{i+\frac{1}{2}}^j - u_{i-\frac{1}{2}}^j \right) \right] \\
 & - \rho_i g \frac{(H_{i+1}^j + H_i^j)}{2} \frac{(H_{i+1}^j - H_i^j)}{\Delta x} = 0.
 \end{aligned} \tag{A14}$$

Parameterization of basal hydrology near grounding lines

G. R. Leguy et al.

Title Page	
Abstract	Introduction
Conclusions	References
Tables	Figures
◀	▶
◀	▶
Back	Close
Full Screen / Esc	
Printer-friendly Version	
Interactive Discussion	



The boundary conditions, Eqs. (A3), (A4) and (A6), are expressed as

$$u_{\frac{3}{2}}^j = 0, \quad (\text{A15})$$

$$\frac{(H_2^j - b_2 - H_1^j + b_1)}{\Delta x} = 0, \quad (\text{A16})$$

$$\frac{1}{\Delta x^{\frac{1}{n}}} 2A^{-\frac{1}{n}} \left| u_{N+M+\frac{1}{2}}^j - u_{N+M-\frac{1}{2}}^j \right|^{\frac{1}{n}-1} \left(u_{N+M+\frac{1}{2}}^j - u_{N+M-\frac{1}{2}}^j \right) - \frac{1}{2} \rho_i \left(1 - \frac{\rho_i}{\rho_w} \right) g H_{N+M}^j = 0, \quad (\text{A17})$$

We solve the stress–balance equation for $u_{i+1/2}^{j+1}$ and the continuity equation for H_i^{j+1} using Picard fixed-point iteration. We use the thickness and velocity from the previous time step as the initial guesses:

$$H_i^{j,0} \equiv H_i^{j-1}, \quad (\text{A18})$$

$$u_{i+1/2}^{j,0} \equiv u_{i+1/2}^{j-1}, \quad (\text{A19})$$

At each iteration, we first solve for the new velocity $u_{i+1/2}^{j,k+1}$ from the stress-balance equation using the “iterate on viscosity” method which can be found in Goldberg et al. (2009). The longitudinal stress at iteration $k + 1$ is defined as

$$\tau_{i,i+\frac{1}{2}}^{j,k+1} \equiv \frac{1}{\Delta x^2} \left[H_{i+1}^{j,k} v_{i+1}^{j,k} \left(u_{i+\frac{3}{2}}^{j,k+1} - u_{i+\frac{1}{2}}^{j,k+1} \right) - H_i^{j,k} v_i^{j,k} \left(u_{i+\frac{1}{2}}^{j,k+1} - u_{i-\frac{1}{2}}^{j,k+1} \right) \right], \quad (\text{A20})$$

$$v_i^{j,k} \equiv \frac{2A^{-\frac{1}{n}}}{\Delta x^{\frac{1}{n}-1}} \left| u_{i+\frac{1}{2}}^{j,k} - u_{i-\frac{1}{2}}^{j,k} \right|^{\frac{1}{n}-1}. \quad (\text{A21})$$

The basal-friction law at iteration $k + 1$ in the ice sheet is given by

$$\tau_{b,i+\frac{1}{2}}^{j,k+1} \equiv -C \left| u_{i+\frac{1}{2}}^{j,k} \right|^{\frac{1}{n}-1} \left[\frac{\left(\frac{\mathcal{N}_{i+1}^{j,k} + \mathcal{N}_i^{j,k}}{2} \right)^n}{\kappa \left| u_{i+\frac{1}{2}}^{j,k} \right| + \left(\frac{\mathcal{N}_{i+1}^{j,k} + \mathcal{N}_i^{j,k}}{2} \right)^n} \right]^{\frac{1}{n}} u_{i+\frac{1}{2}}^{j,k+1}, \quad (\text{A22})$$

and similarly for the cell containing the grounding line. Basal stress in the ice shelf is zero for all iterations. Driving stress does not depend explicitly on u ; it is computed entirely from time-independent quantities or thicknesses at iteration k . Boundary conditions are

$$u_{\frac{3}{2}}^{j,k+1} = 0, \quad (\text{A23})$$

$$\frac{1}{\Delta x} v_{N+M}^{j,k} \left(u_{N+M+\frac{1}{2}}^{j,k+1} - u_{N+M-\frac{1}{2}}^{j,k+1} \right) = \frac{1}{2} \rho_i \left(1 - \frac{\rho_i}{\rho_w} \right) g H_{N+M}^{j,k}. \quad (\text{A24})$$

The result is a linear system involving a tridiagonal matrix

$$\mathbf{M}_u^k u^{k+1} = r_u^k. \quad (\text{A25})$$

We use a sparse matrix solver to compute the new velocities.

Then, we solve the continuity equation for the new thicknesses $H_i^{j,k+1}$:

$$\frac{H_i^{j,k+1} - H_i^{j-1}}{\Delta t} + \theta \mathcal{F}_i^{j,k+1} + (1 - \theta) \mathcal{F}_i^{j-1} = a, \quad (\text{A26})$$

where

$$\mathcal{F}_i^{j,k+1} \equiv \frac{\left(H_{\text{up},i+\frac{1}{2}}^{j,k+1} u_{i+\frac{1}{2}}^{j,k+1} - H_{\text{up},i-\frac{1}{2}}^{j,k+1} u_{i-\frac{1}{2}}^{j,k+1} \right)}{\Delta x}, \quad (\text{A27})$$

Parameterization of basal hydrology near grounding lines

G. R. Leguy et al.

Title Page

Abstract

Introduction

Conclusions

References

Tables

Figures

◀

▶

◀

▶

Back

Close

Full Screen / Esc

Printer-friendly Version

Interactive Discussion



and where

$$H_{\text{up},i+\frac{1}{2}}^{j,k+1} \equiv \begin{cases} H_i^{j,k+1} \text{ if } u_{i+\frac{1}{2}}^{j,k+1} \geq 0, \\ H_{i+1}^{j,k+1} \text{ if } u_{i+\frac{1}{2}}^{j,k+1} \leq 0. \end{cases} \quad (\text{A28})$$

The boundary condition here is

$$H_2^{j,k+1} - H_1^{j,k+1} = b_2 - b_1. \quad (\text{A29})$$

The tridiagonal linear system (actually u is typically strictly positive so the system is bidiagonal) is solved for the new thickness.

$$\mathbf{M}_H^{k+1} \mathbf{H}^{k+1} = \mathbf{r}_H. \quad (\text{A30})$$

10 Iteration continues until the the residual

$$R^k \equiv \mathbf{M}_u^k \mathbf{u}^k - \mathbf{r}_u^k < 10^{-10} \max \left(\left| \tau_{d,i+\frac{1}{2}}^{j,k} \right| \right). \quad (\text{A31})$$

Note that all terms are evaluated at iteration k .

A2 Addition of the GLP

15 A few simple modifications to the numerical method from the previous section are required to add a grounding-line parameterization (GLP), as defined in Gladstone et al. (2010a). The basal and driving stresses in the grid cell containing the grounding line are modified so that the stresses transition smoothly between their grounded and floating values as the grounding line passes through the cell. Following Pattyn et al.
 20 (2006), we define the grounding-line position to be the location where the function

Parameterization of basal hydrology near grounding lines

G. R. Leguy et al.

Title Page

Abstract

Introduction

Conclusions

References

Tables

Figures

◀

▶

◀

▶

Back

Close

Full Screen / Esc

Printer-friendly Version

Interactive Discussion



$f_{\text{Pattyn}}(x) = H_i(x)/H(x)$ is equal to one. Values of f_{Pattyn} at arbitrary x values are computed by linear interpolation between values at H -grid points:

$$f_{\text{Pattyn}}(x) = \left(1 - \frac{x - x_i}{\Delta x}\right) f_i + \left(\frac{x - x_i}{\Delta x}\right) f_{i+1} \quad x_i \leq x < x_{i+1}, \quad (\text{A32})$$

$$f_i \equiv H_i(x_i)/H_i. \quad (\text{A33})$$

With this definition, the grounding-line position x_g is given by

$$f_{\text{Pattyn}}(x_g) \equiv 1, \quad (\text{A34})$$

$$x_g = x_i + \frac{1 - f_i}{f_{i+1} - f_i} \Delta x. \quad (\text{A35})$$

Following Gladstone et al. (2010a), we define the fraction of the u -grid cell that is grounded as:

$$\lambda_g \equiv \frac{1 - f_i}{f_{i+1} - f_i}. \quad (\text{A36})$$

Assuming the u -grid cell at $N + 1/2$ contains the grounding line, the three stresses at the center of this cell are

$$\tau_{l,N+1/2} = \frac{2A^{-1/n}}{\Delta x^{1+1/n}} \left[H_{N+1}^j \left| u_{N+3/2}^j - u_{N+1/2}^j \right|^{1/n-1} \left(u_{N+3/2}^j - u_{N+1/2}^j \right) - H_N^j \left| u_{N+1/2}^j - u_{N-1/2}^j \right|^{1/n-1} \left(u_{N+1/2}^j - u_{N-1/2}^j \right) \right], \quad (\text{A37})$$

$$\tau_{b,N+1/2} = -\lambda_g C \left| u_{N+1/2}^j \right|^{1/n-1} u_{N+1/2}^j \left[\frac{\left(\frac{\mathcal{N}_{N+1}^j + \mathcal{N}_N^j}{2} \right)^n}{\kappa \left| u_{N+1/2}^j \right| + \left(\frac{\mathcal{N}_{N+1}^j + \mathcal{N}_N^j}{2} \right)^n} \right]^{1/n}, \quad (\text{A38})$$

Parameterization of basal hydrology near grounding lines

G. R. Leguy et al.

Title Page	
Abstract	Introduction
Conclusions	References
Tables	Figures
◀	▶
◀	▶
Back	Close
Full Screen / Esc	
Printer-friendly Version	
Interactive Discussion	



$$\tau_{d,N+\frac{1}{2}} = -\rho_i g \frac{(H_{N+1}^j + H_N^j)}{2} \left[\lambda_g \frac{(H_{N+1}^j - b_{N+1} - H_N^j + b_N)}{\Delta x} + (1 - \lambda_g) \delta \frac{(H_{N+1}^j - H_N^j)}{\Delta x} \right], \quad (\text{A39})$$

where, as usual, the stresses must balance:

$$\tau_{l,N+\frac{1}{2}} + \tau_{b,N+\frac{1}{2}} + \tau_{d,N+\frac{1}{2}} = 0. \quad (\text{A40})$$

Note that τ_l has not been modified as part of the GLP because longitudinal stress takes the same form in the ice sheet and the ice shelf. The other equations of the system are unchanged from the previous section.

10 A3 Chebyshev model

The Chebyshev model is a Python code that finds steady-state solutions to the equations of motion. The code is pseudo-spectral (Boyd, 2001): integrals and derivatives are computed in *spectral space* (i.e., using Chebyshev modes), whereas products and quotients are computed in *physical space* on a collocation grid. The collocation points
15 are the Chebyshev–Gauss–Lobatto nodes, defined as:

$$x_k = x_g \frac{1 - \cos\left(\frac{\pi k}{N}\right)}{2} \quad k = 0, 1, \dots, N, \quad (\text{A41})$$

where $N = 1024$ is the order of the Chebyshev polynomials that form the set of basis functions. This choice of collocation grids means that there are collocation points on the domain boundaries – the ice divide ($x_0 = 0$) and the grounding line ($x_N = x_g$) – which makes applying boundary conditions at these locations relatively straightforward. We
20

used open-source code from PyBlog (von Winkel, 2013) for transformations between physical and spectral space and for recurrence relations for integrals and derivatives.

The code uses the derivative of thickness, H_x , as its primary computational variable. This choice reduces numerical noise because we never need to compute the second derivative of the primary variable. Higher-order derivatives introduce increasing amounts of numerical noise, whereas integrals tend to remove noise. The thickness H is derived from H_x by integration

$$H = H(x_g) + \int_{x_g}^x H_x dx', \quad (\text{A42})$$

where $H(x_g)$ is known from the flotation boundary condition, Eq. (9). The velocity u is determined from H using the integral of the steady-state continuity equation, $uH = a x$, and the velocity derivative u_x is computed from the continuity equation, Eq. (1), with $H_t \equiv 0$:

$$u = \frac{a x}{H}, \quad (\text{A43})$$

$$u_x = \frac{a + uH_x}{H}. \quad (\text{A44})$$

Given u , H and their derivatives, we use Picard iteration to solve stress-balance, Eq. (2). Each Picard iteration involves solving the following linear system for $H_{x,k+1}$, based on the results computed at the previous iteration k :

$$\mathbf{M}_k \mathbf{H}_{x,k+1} = \mathbf{c}_k, \quad (\text{A45})$$

$$\mathbf{M} \equiv -\mathcal{D}(\mathbf{v}_{x,k} \mathbf{u}_k + \mathbf{v}_{-k} \mathbf{u}_{x,k} + \mathbf{H}_k) - \mathcal{D}(\mathbf{v}_k \mathbf{u}_k) \cdot \mathbf{D}_x, \quad (\text{A46})$$

$$\mathbf{c}_k \equiv -\mathbf{v}_{x,k} a - \boldsymbol{\tau}_{b,k} - \mathbf{H}_k \mathbf{b}_{x,k}, \quad (\text{A47})$$

$$\mathbf{v} \equiv 2\bar{A}^{-\frac{1}{n}} |u_x|^{\frac{1}{n}-1}, \quad (\text{A48})$$

Parameterization of basal hydrology near grounding lines

G. R. Leguy et al.

Title Page

Abstract

Introduction

Conclusions

References

Tables

Figures

◀

▶

◀

▶

Back

Close

Full Screen / Esc

Printer-friendly Version

Interactive Discussion



where quantities in bold italics are vectors of $N + 1$ values from each collocation point, quantities that are bold and in capital letters are $(N + 1) \times (N + 1)$ matrices, \mathcal{D} is an operator that puts the vector elements along the diagonal of a matrix, \mathbf{D}_x is the Chebyshev derivative operator expressed as a matrix, and $\tau_{b,k}$ is given by Eq. (6) with all quantities evaluated at iteration k . Products of vectors are defined element-wise in these equations, rather than as dot products. Picard iteration requires an initial guess at H_x , which we define as

$$H_{x,0} \equiv 2 [H(x_g) - H_0] \frac{x}{x_g^2}, \quad (\text{A49})$$

$$H_0 \equiv 3000 \text{ m}. \quad (\text{A50})$$

An outer iterative loop uses Brent's root-finding method (Brent, 1973) to find the grounding-line position x_g where the final boundary condition, Eq. (13), is satisfied. Brent's method requires bounds on x_g : we break the domain into segments of downward-sloping bedrock topography and search for steady states independently on each segment. The method is also capable of finding unstable steady states on upward-sloping bedrock. The method is considered to have converged when both the residual $r = \max(|\mathbf{M}_k \mathbf{H}_{x,k} - \mathbf{c}_k|)$ and the residual in Eq. (13) are less than 10^{-10} . All computational variables are non-dimensionalized to be of order unity.

Acknowledgements. This work was supported by the Earth System Modeling and Scientific Discovery through Advanced Computing (SciDAC) programs funded by the US Department of Energy, Office of Science, Biological and Environmental Research and Advanced Scientific Computing Research. The Los Alamos National Laboratory is operated by the DOE National Nuclear Security Administration under Contract DE-AC52-06NA25396. The authors would like to thank Christian Schoof, Matt Hoffman, Steve Price and Ed Bueler for fruitful conversation. The authors also thank the editor, Olivier Gagliardini, for his comments that have improved the quality of the paper.

Parameterization of basal hydrology near grounding lines

G. R. Leguy et al.

Title Page

Abstract

Introduction

Conclusions

References

Tables

Figures

◀

▶

◀

▶

Back

Close

Full Screen / Esc

Printer-friendly Version

Interactive Discussion



References

- Boyd, J.: Chebyshev and Fourier Spectral Methods, Dover Books on Mathematics Series, Dover Publ., New York, 2001. 376, 398
- Brent, R.: Algorithms for Minimization without Derivatives, Prentice-Hall, Englewood Cliffs, New Jersey, 1973. 400
- 5 Budd, W. F. and Jenssen, D.: The dynamics of the Antarctic ice sheet, *Ann. Glaciol.*, 12, 16–22, 1989. 367
- Budd, W. F., Keage, P. L., and Blundy, N. A.: Empirical studies of ice sliding, *J. Glaciol.*, 23, 157–170, 1979. 367
- 10 Bueler, E. and Brown, J.: Shallow shelf approximation as a “sliding law” in a thermomechanically coupled ice sheet model, *J. Geophys. Res.-Earth*, 114, F03008, doi:10.1029/2008JF001179, 2009. 365, 367
- Carter, S. P. and Fricker, H. A.: The supply of subglacial meltwater to the grounding line of the Siple Coast, West Antarctica, *Ann. Glaciol.*, 53, 267–280, 2012. 366, 367
- 15 Cornford, S. L., Martin, D. F., Graves, D. T., Ranken, D. F., Brocq, A. M. L., Gladstone, R. M., Payne, A. J., Ng, E. G., and Lipscomb, W. H.: Adaptive mesh, finite volume modeling of marine ice sheets, *J. Comput. Phys.*, 232, 529–549, 2013. 365, 366, 381, 387
- Cuffey, K. and Paterson, W. S. B.: *The Physics of Glaciers*, Academic Press, 2010. 367, 387
- Durand, G., Gagliardini, O., de Fleurian, B., Zwinger, T., and Le Meur, E.: Marine ice sheet dynamics: hysteresis and neutral equilibrium, *J. Geophys. Res.-Earth*, 114, F03009, doi:10.1029/2008JF001170, 2009. 364, 365, 366, 379
- 20 Favier, L., Gagliardini, O., Durand, G., and Zwinger, T.: A three-dimensional full Stokes model of the grounding line dynamics: effect of a pinning point beneath the ice shelf, *The Cryosphere*, 6, 101–112, doi:10.5194/tc-6-101-2012, 2012. 364, 387
- 25 Fricker, H. A. and Scambos, T.: Connected subglacial lake activity on lower Mercer and Whillans Ice Streams, West Antarctica, 2003–2008, *J. Glaciol.*, 55, 303–315, 2009. 367
- Fricker, H. A., Coleman, R., Padman, L., Scambos, T. A., Bohlander, J., and Brunt, K. M.: Mapping the grounding zone of the Amery Ice Shelf, East Antarctica using InSAR, MODIS and ICESat, *Antarct. Sci.*, 21, 515–532, 2009. 367
- 30 Gagliardini, O., Cohen, D., Raaback, P., and Zwinger, T.: Finite-element modeling of subglacial cavities and related friction law, *J. Geophys. Res.-Earth*, 112, F02027, doi:10.1029/2006JF000576, 2007. 370, 371, 372

Parameterization of basal hydrology near grounding lines

G. R. Leguy et al.

Title Page

Abstract

Introduction

Conclusions

References

Tables

Figures

◀

▶

◀

▶

Back

Close

Full Screen / Esc

Printer-friendly Version

Interactive Discussion



Parameterization of basal hydrology near grounding lines

G. R. Leguy et al.

Title Page

Abstract

Introduction

Conclusions

References

Tables

Figures

◀

▶

◀

▶

Back

Close

Full Screen / Esc

Printer-friendly Version

Interactive Discussion



Gladstone, R. M., Payne, A. J., and Cornford, S. L.: Parameterising the grounding line in flow-line ice sheet models, *The Cryosphere*, 4, 605–619, doi:10.5194/tc-4-605-2010, 2010a. 365, 375, 376, 379, 381, 387, 396, 397

Gladstone, R. M., Lee, V., Vieli, A., and Payne, A. J.: Grounding line migration in an adaptive mesh ice sheet model, *J. Geophys. Res.-Earth*, 115, F04014, doi:10.1029/2009JF001615, 2010b. 365, 366

Goldberg, D., Holland, D. M., and Schoof, C.: Grounding line movement and ice shelf buttressing in marine ice sheets, *J. Geophys. Res.*, 114, F04026, doi:10.1029/2008JF001227, 2009. 366, 387, 388, 394

Hindmarsh, R. C. A.: A numerical comparison of approximations to the Stokes equations used in ice sheet and glacier modeling, *J. Geophys. Res.-Earth*, 109, 1–15, 2004. 365

Holland, P. R.: A model of tidally dominated ocean processes near ice shelf grounding lines, *J. Geophys. Res.-Oceans*, 113, C11002, doi:10.1029/2007JC004576, 2008. 367

Joughin, I. and Alley, R. B.: Stability of the West Antarctic ice sheet in a warming world, *Nat. Geosci.*, 4, 506–513, 2011. 364

Larour, E., Schiermeier, J., Rignot, E., Seroussi, H., Morlighem, M., and Paden, J.: Sensitivity analysis of Pine Island Glacier ice flow using ISSM and DAKOTA, *J. Geophys. Res.-Earth*, 117, F02009, doi:10.1029/2011JF002146, 2012. 388

Le Brocq, A. M., Ross, N., Griggs, J. A., Bingham, R. G., Corr, H. F., Ferraccioli, F., Jenkins, A., Jordan, T. A., Payne, A. J., and Rippin, D. M.: Evidence from ice shelves for channelized meltwater flow beneath the Antarctic Ice Sheet, *Nat. Geosci.*, 6, 945–948, 2013. 367

Lipscomb, W. H., Fyke, J. G., Vizcaino, M., Sacks, W. J., Wolfe, J., Vertenstein, M., Craig, A., Kluzek, E., and Lawrence, D. M.: Implementation and initial evaluation of the Glimmer Community Ice Sheet Model in the Community Earth System Model, *J. Climate*, 26, 7352–7371, doi:10.1175/JCLI-D-12-00557.1, 2013. 389

MacAyeal, D. R.: Large-scale ice flow over a viscous basal sediment: theory and application to ice stream B, Antarctica, *J. Geophys. Res.-Sol. Ea.*, 94, 4071–4087, 1989. 365, 369

Makinson, K., King, M. A., Nicholls, K. W., and Gudmundsson, G. H.: Diurnal and semidiurnal tide-induced lateral movement of Ronne Ice Shelf, Antarctica, *Geophys. Res. Lett.*, 39, L10501, doi:10.1029/2012GL051636, 2012. 367

Martin, M. A., Winkelmann, R., Haseloff, M., Albrecht, T., Bueler, E., Khroulev, C., and Levermann, A.: The Potsdam Parallel Ice Sheet Model (PISM-PIK) – Part 2: Dynamic equilibrium

Parameterization of basal hydrology near grounding lines

G. R. Leguy et al.

Title Page

Abstract

Introduction

Conclusions

References

Tables

Figures

◀

▶

◀

▶

Back

Close

Full Screen / Esc

Printer-friendly Version

Interactive Discussion



simulation of the Antarctic ice sheet, *The Cryosphere*, 5, 727–740, doi:10.5194/tc-5-727-2011, 2011. 366, 367

Muszynski, I. and Birchfield, G. E.: A coupled marine ice-stream–ice-shelf model, *J. Glaciol.*, 33, 3–15, 1987. 365, 368

5 Pattyn, F.: A new three-dimensional higher-order thermomechanical ice sheet model: basic sensitivity, ice stream development, and ice flow across subglacial lakes, *J. Geophys. Res.-Sol. Ea.*, 108, 2382, doi:10.1029/2002JB002329, 2003. 365

Pattyn, F., Huyghe, A., De Brabander, S., and De Smedt, B.: Role of transition zones in marine ice sheet dynamics, *J. Geophys. Res.-Earth*, 111, F02004, doi:10.1029/2002JB002329, 2006. 365, 366, 373, 375, 396

10 Pattyn, F., Schoof, C., Perichon, L., Hindmarsh, R. C. A., Bueler, E., de Fleurian, B., Durand, G., Gagliardini, O., Gladstone, R., Goldberg, D., Gudmundsson, G. H., Huybrechts, P., Lee, V., Nick, F. M., Payne, A. J., Pollard, D., Rybak, O., Saito, F., and Vieli, A.: Results of the Marine Ice Sheet Model Intercomparison Project, MISMP, *The Cryosphere*, 6, 573–588, doi:10.5194/tc-6-573-2012, 2012. 365, 375, 377, 378, 379, 382, 383, 407, 408

15 Perego, M., Gunzburger, M., and Burkardt, J.: Parallel finite-element implementation for higher-order ice-sheet models, *J. Glaciol.*, 58, 76–88, 2012. 365, 387, 389

Pimentel, S., Flowers, G. E., and Schoof, C. G.: A hydrologically coupled higher-order flow-band model of ice dynamics with a Coulomb friction sliding law, *J. Geophys. Res.-Earth*, 115, F04023, doi:10.1029/2002JB002329, 2010. 367

20 Rignot, E., Velicogna, I., Van den Broeke, M. R., Monaghan, A., and Lenaerts, J.: Acceleration of the contribution of the Greenland and Antarctic ice sheets to sea level rise, *Geophys. Res. Lett.*, 38, L05503, doi:10.1029/2011GL046583, 2011. 364

Rutt, I. C., Hagdorn, M., Hulton, N. R. J., and Payne, A. J.: The Glimmer community ice sheet model, *J. Geophys. Res.-Earth*, 114, F02004, doi:10.1029/2011GL046583, 2009. 365, 389

25 Schoof, C.: The effect of cavitation on glacier sliding, *P. R. Soc. A*, 461, 609–627, doi:doi:10.1098/rspa.2004.1350, 2005. 367, 369, 370, 371, 372

Schoof, C.: Ice sheet grounding line dynamics: steady states, stability, and hysteresis, *J. Geophys. Res.*, 112, F03S28, doi:10.1029/2006JF000664, 2007a. 364, 365, 366, 368, 369, 370, 371, 374, 376, 377, 378, 379, 382, 383, 388, 415

30 Schoof, C.: Marine ice-sheet dynamics – Part 1: The case of rapid sliding, *J. Fluid Mech.*, 573, 27–55, 2007b. 379, 411, 412

Parameterization of basal hydrology near grounding lines

G. R. Leguy et al.

Title Page

Abstract

Introduction

Conclusions

References

Tables

Figures

◀

▶

◀

▶

Back

Close

Full Screen / Esc

Printer-friendly Version

Interactive Discussion



- Schoof, C. and Hindmarsh, R. C.: Thin-film flows with wall slip: an asymptotic analysis of higher order glacier flow models, *Q. J. Mech. Appl. Math.*, 63, 73–114, 2010. 365
- Tulaczyk, S., Kamb, W. B., and Engelhardt, H. F.: Basal mechanics of Ice Stream B, West Antarctica: 1. Till mechanics, *J. Geophys. Res.-Sol. Ea.*, 105, 463–481, 2000a. 366
- 5 Tulaczyk, S., Kamb, W. B., and Engelhardt, H. F.: Basal mechanics of Ice Stream B, West Antarctica: 2. Undrained plastic bed model, *J. Geophys. Res.-Sol. Ea.*, 105, 483–494, 2000b. 366, 373
- van der Wel, N., Christoffersen, P., and Bougamont, M.: The influence of subglacial hydrology on the flow of Kamb Ice Stream, West Antarctica, *J. Geophys. Res.-Earth*, 118, 97–110, doi:10.1029/2012JF002570, 2013. 366, 373, 388
- 10 Vaughan, D. G. and Spouge, J. R.: Risk estimation of collapse of the West Antarctic ice sheet, *Climatic Change*, 52, 65–91, 2002. 364
- Velicogna, I.: Increasing rates of ice mass loss from the Greenland and Antarctic ice sheets revealed by GRACE, *Geophys. Res. Lett.*, 36, L19503, doi:10.1029/2009GL040222, 2009. 364
- 15 Vieli, A. and Payne, A. J.: Application of control methods for modelling the flow of Pine Island Glacier, West Antarctica, *Ann. Glaciol.*, 36, 197–204, 2003. 388
- Vieli, A. and Payne, A. J.: Assessing the ability of numerical ice sheet models to simulate grounding line migration, *J. Geophys. Res.-Earth*, 110, F01003, doi:10.1029/2004JF000202, 2005. 365, 375, 387
- 20 von Winkel, G.: PyBlog, available at: <http://www.scientificpython.net/pyblog.html> (last access: 30 September 2013), 2013. 399
- Weertman, J.: Stability of the junction of an ice sheet and an ice shelf, *J. Glaciol.*, 13, 3–11, 1974. 364, 382
- 25 Whillans, I. M. and Veen, C. J.: The role of lateral drag in the dynamics of Ice Stream B, Antarctica, *J. Glaciol.*, 43, 231–237, 1997. 388
- Wingham, D. J., Siegert, M. J., Shepherd, A., and Muir, A. S.: Rapid discharge connects Antarctic subglacial lakes, *Nature*, 440, 1033–1036, 2006. 367

Parameterization of basal hydrology near grounding lines

G. R. Leguy et al.

Title Page

Abstract

Introduction

Conclusions

References

Tables

Figures



Back

Close

Full Screen / Esc

Printer-friendly Version

Interactive Discussion



Table 1. Model variables.

Variables	Units	Definition
H	km	Ice thickness
u	m a^{-1}	Ice velocity
b	km	Ice sheet bed elevation, positive downward
s	km	Surface elevation
x_g	km	Horizontal grounding line position

Parameterization of basal hydrology near grounding lines

G. R. Leguy et al.

Table 2. Parameter values used for all experiments.

Parameters	Value	Units	Definition
ρ_i	916	kg m^{-3}	Ice density
ρ_w	1000	kg m^{-3}	Water density
A	see tables	$\text{Pa}^{-3} \text{s}^{-1}$	Ice softness
A_b	3.1688×10^{-24}	$\text{Pa}^{-3} \text{s}^{-1}$	Ice softness at the bed
C	7.62×10^6	$\text{Pa} (\text{m}^{-1} \text{s})^{1/3}$	Shear stress factor
a	0.3	m a^{-1}	Ice accumulation rate
g	9.81	m s^{-2}	Gravitational acceleration
n	3	–	Glen's flaw law exponent
m_{max}	0.5	–	Maximum bed obstacle slope
λ_{max}	2	m	Wavelength of bedrock bumps

Title Page

Abstract

Introduction

Conclusions

References

Tables

Figures

◀

▶

◀

▶

Back

Close

Full Screen / Esc

Printer-friendly Version

Interactive Discussion



Parameterization of basal hydrology near grounding lines

G. R. Leguy et al.

Title Page

Abstract

Introduction

Conclusions

References

Tables

Figures

◀

▶

◀

▶

Back

Close

Full Screen / Esc

Printer-friendly Version

Interactive Discussion



Table 3. Values of the ice softness A used in the MISMIP experiment 1 (linear bed). These are the same values prescribed in Pattyn et al. (2012).

Step no.	$A (\times 10^{-26} \text{ s}^{-1} \text{ Pa}^{-3})$
1	464.16
2	215.44
3	100
4	46.416
5	21.544
6	10
7	4.6416
8	2.1544
9	1

Table 4. Values of the ice softness A used in the MISMIP experiment 3 (polynomial bed). The range given for $p = 0$, $p = 0.25$, $p = 0.5$ corresponds to the range given in Pattyn et al. (2012). The additional values of A for larger values of p are necessary for the grounding line to cross through the unstable region.

Step no.	$A (\times 10^{-26} \text{ s}^{-1} \text{ Pa}^{-3})$	
	$p = \{0, 0.25, 0.5\}$	$p = \{0.75, 1\}$
1	30	30
2	25	25
3	20	20
4	15	15
5	10	10
6	5	5
7	2.5	2.5
8	5	2
9	10	1.5
10	15	1
11	20	0.5
12	25	0.25
13	30	0.5
14	–	1
15	–	1.5
16	–	2
17	–	2.5
18	–	5
19	–	10
20	–	15
21	–	20
22	–	25
23	–	30

Parameterization of basal hydrology near grounding lines

G. R. Leguy et al.

Title Page

Abstract Introduction

Conclusions References

Tables Figures

◀ ▶

◀ ▶

Back Close

Full Screen / Esc

Printer-friendly Version

Interactive Discussion



Parameterization of basal hydrology near grounding lines

G. R. Leguy et al.

Table 5. Aggregate measures of the error in grounding-line position for the ten experiments at 3.2, 1.6 and 0.8 km resolution over the linear bed. The “Max err” is the maximum error over the advance and retreat experiments. The “FMI” (final minus initial) error is the difference between the final and initial errors over the whole experiment. When expressed as a percentage, the measure is the error divided by the total change in grounding-line position between the most advanced and the most retreated states using the benchmark model.

Grounding-line position metrics for linear bed									
Resolution km	p values	No GLP				With GLP			
		Max err km	Max err %	FMI km	FMI %	Max err km	Max err %	FMI km	FMI %
3.2	0	530	77	590	86	64	9.2	120	18
	0.25	460	65	500	71	58	8.3	110	15
	0.5	260	36	260	36	72	10	72	10
	0.75	110	17	78	12	75	12	31	4.8
	1	51	10	14	2.7	58	11	15	2.7
1.6	0	360	52	400	58	42	6.1	81	12
	0.25	270	38	300	42	36	5.1	65	9.2
	0.5	120	16	110	16	43	6.1	38	5.3
	0.75	47	7.4	26	4.1	45	7.1	22	3.4
	1	23	4.2	2.6	0.5	30	5.6	22	2.3
0.8	0	220	32	240	35	28	4.1	51	7.3
	0.25	120	18	130	19	22	5.1	41	5.8
	0.5	50	7.1	48	6.8	29	4.1	27	3.8
	0.75	19	3.0	6.9	1.1	24	3.8	14	2.2
	1	10	1.9	$\leq 10^{-3}$	$\leq 10^{-3}$	15	2.8	6.1	1.1



Parameterization of basal hydrology near grounding lines

G. R. Leguy et al.

Table 6. Aggregate measures of the error as Table 5, but over a polynomial bed.

Grounding-line position metrics for polynomial bed									
Resolution km	p values	No GLP				With GLP			
		Max err km	Max err %	FMI km	FMI %	Max err km	Max err %	FMI km	FMI %
3.2	0	700	99	690	97	610	86	580	81
	0.25	710	99	700	97	610	85	570	80
	0.5	700	95	660	90	620	84	3.0	0.4
	0.75	610	73	$\leq 10^{-3}$	$\leq 10^{-3}$	580	70	$\leq 10^{-3}$	$\leq 10^{-3}$
	1	60	7.2	$\leq 10^{-3}$	$\leq 10^{-3}$	73	8.8	$\leq 10^{-3}$	$\leq 10^{-3}$
1.6	0	710	100	680	95	600	84	550	78
	0.25	710	99	690	96	590	81	1.5	0.2
	0.5	640	87	600	81	590	80	$\leq 10^{-3}$	$\leq 10^{-3}$
	0.75	44	5.4	12	1.4	38	4.6	6.0	0.7
	1	530	63	1.2	0.1	50	6.0	1.4	0.2
0.8	0	680	96	650	91	580	81	$\leq 10^{-3}$	$\leq 10^{-3}$
	0.25	660	91	640	89	45	6.3	$\leq 10^{-3}$	$\leq 10^{-3}$
	0.5	590	81	17	2.3	20	2.7	4.6	0.6
	0.75	20	2.4	3.6	0.4	23	2.7	3.8	0.5
	1	29	3.4	$\leq 10^{-3}$	$\leq 10^{-3}$	33	3.9	$\leq 10^{-2}$	$\leq 10^{-3}$

Title Page

Abstract

Introduction

Conclusions

References

Tables

Figures

◀

▶

◀

▶

Back

Close

Full Screen / Esc

Printer-friendly Version

Interactive Discussion



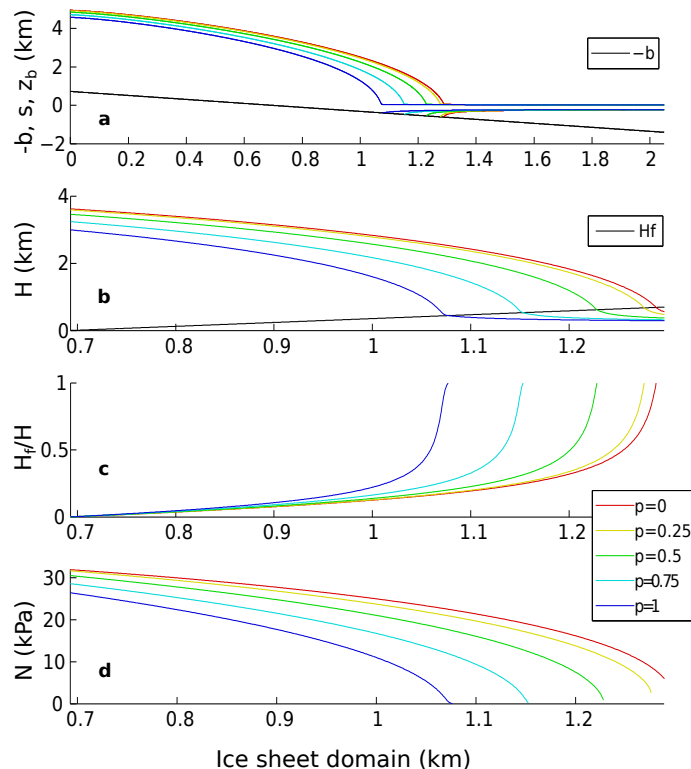


Fig. 1. Dependence of ice geometry and effective pressure on the hydrological-connectivity parameter p over a linear bed as in Schoof (2007b). All panels show the non-GLP fixed-grid solution at 0.8 km resolution and with ice softness $A = 10^{-25} \text{ Pa}^{-3} \text{ s}^{-1}$. **(a)** Ice surface and bedrock, and basal elevation (s , $-b$ and z_b , respectively) over the full ice-sheet domain. **(b)** Ice sheet thickness and height above flotation over the marine portion of the ice sheet. **(c)** The ratio between the flotation thickness and the ice-sheet thickness. **(d)** The effective pressure N , which approaches zero more smoothly with increasing p .

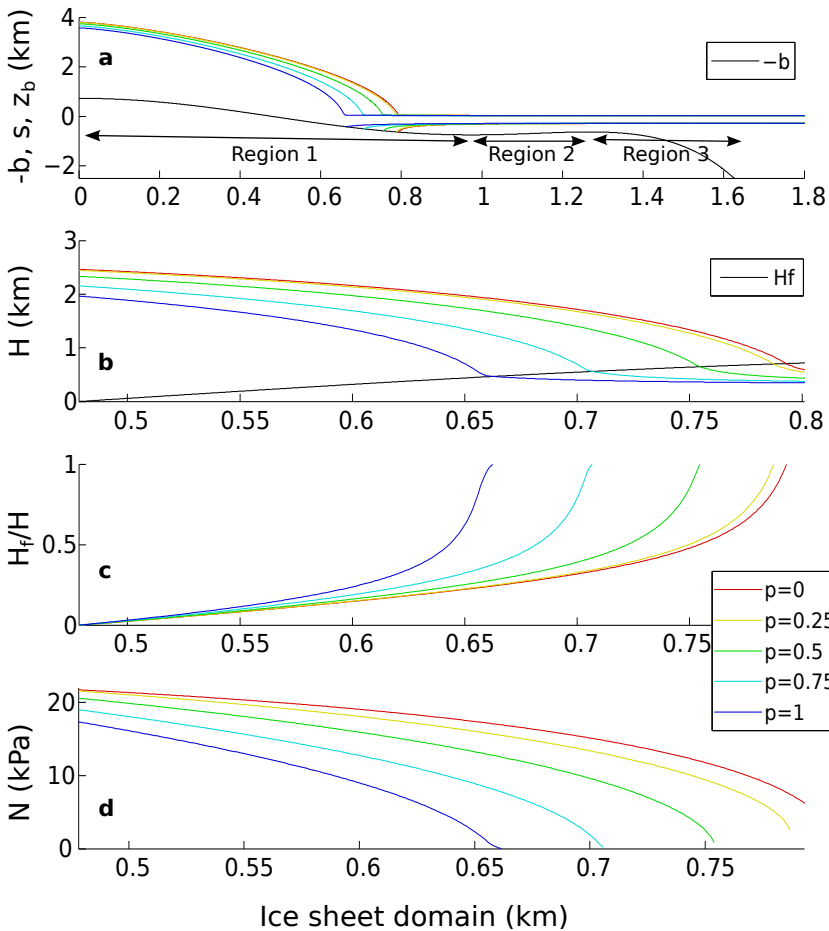


Fig. 2. Dependence of ice geometry and effective pressure on ρ , as in Fig. 1 but with the polynomial bed as in Schoof (2007b), containing two stable regions (1 and 3) and an unstable region (2).

Parameterization of basal hydrology near grounding lines

G. R. Leguy et al.

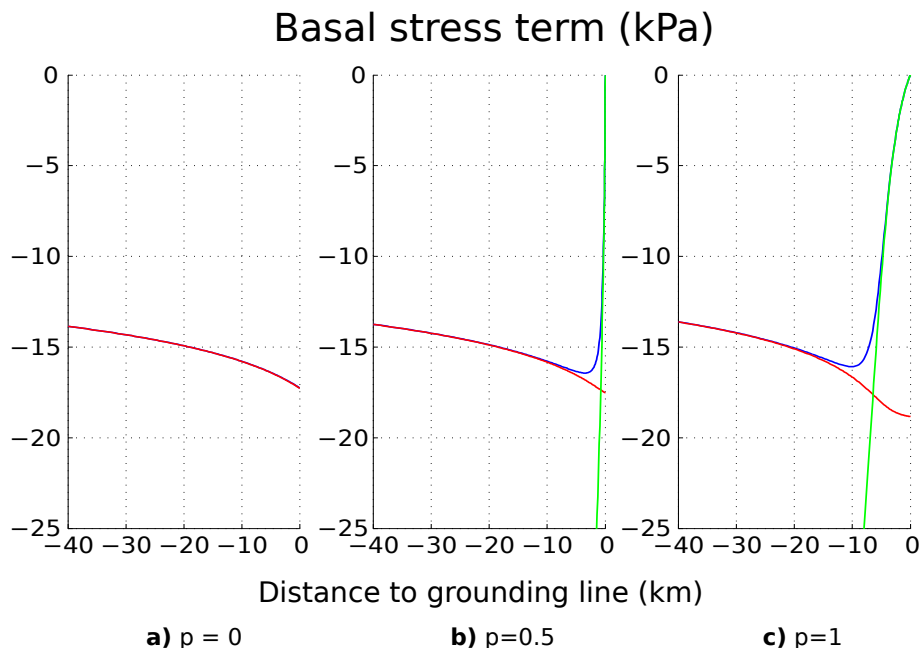


Fig. 3. Basal stress given by Eq. (15) (blue) and its asymptotic limits, Eq. (16) (red) and Eq. (17) (green) for ice softness $A = 10^{-25} \text{ Pa}^{-3} \text{ s}^{-1}$ and using the Chebyshev benchmark solution **(a)**. When $\rho = 0$, the second (green) asymptote is never reached, the red and blue curves overlap almost exactly, and there is no transition zone (basal stress falls abruptly to zero at the grounding line) **(b)** and **(c)**. When $\rho = 0.5$ and $\rho = 1$, the length of the transition zone, defined as the region where $0 \leq N(\rho)^n \leq \kappa u$ (roughly speaking, the region where the blue curve differs from the red curve), ranges from several hundred meters to 20 km depending on A , ρ and bedrock topography.

Parameterization of basal hydrology near grounding lines

G. R. Leguy et al.

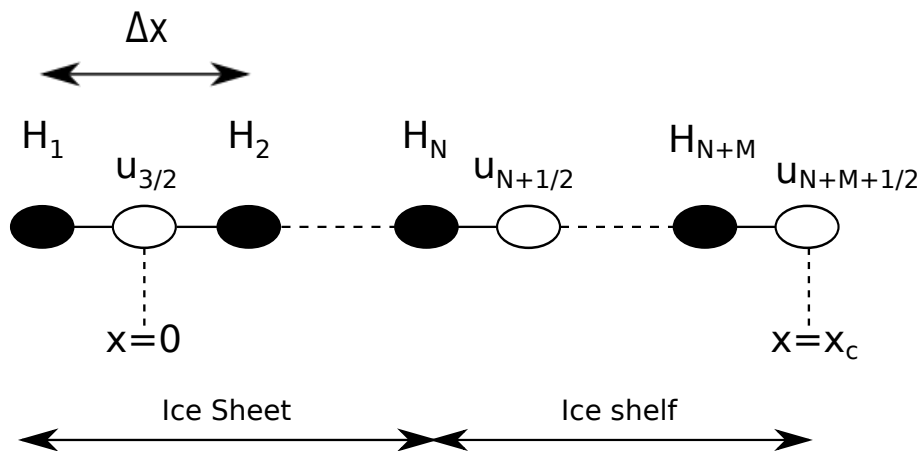


Fig. 4. Illustration of the staggered grid used in the model. The H -grid points are represented by solid circles and the u -grid points by empty circles. Δx is the grid spacing (on both H - and u -grids). H_N is the ice thickness in the last grounded point. The ice divide is at $x = 0$ and the calving front at $x = x_c$.

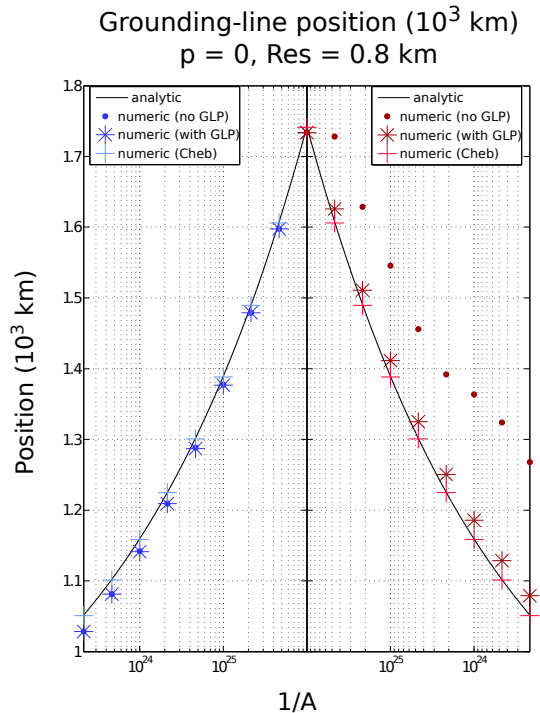


Fig. 5. The grounding-line position during advance and retreat experiments over a linear bed with $p = 0$ from the boundary-layer solution by Schoof (2007a) (solid black), the Chebyshev benchmark model (pluses), the fixed-grid model without the GLP (dots) and the fixed-grid model with the GLP (stars). The boundary-layer solution is in close agreement with the Chebyshev benchmark (maximum difference of 1.2 km), as are the fixed-grid results that include the GLP (maximum difference of 28 km). Without the GLP, the fixed-grid grounding line follows the benchmark relatively closely during advance (maximum error of 22 km) but not during retreat (maximum error of 220 km).

Parameterization of basal hydrology near grounding lines

G. R. Leguy et al.

Title Page

Abstract Introduction

Conclusions References

Tables Figures

◀ ▶

◀ ▶

Back Close

Full Screen / Esc

Printer-friendly Version

Interactive Discussion



Parameterization of
basal hydrology near
grounding lines

G. R. Leguy et al.

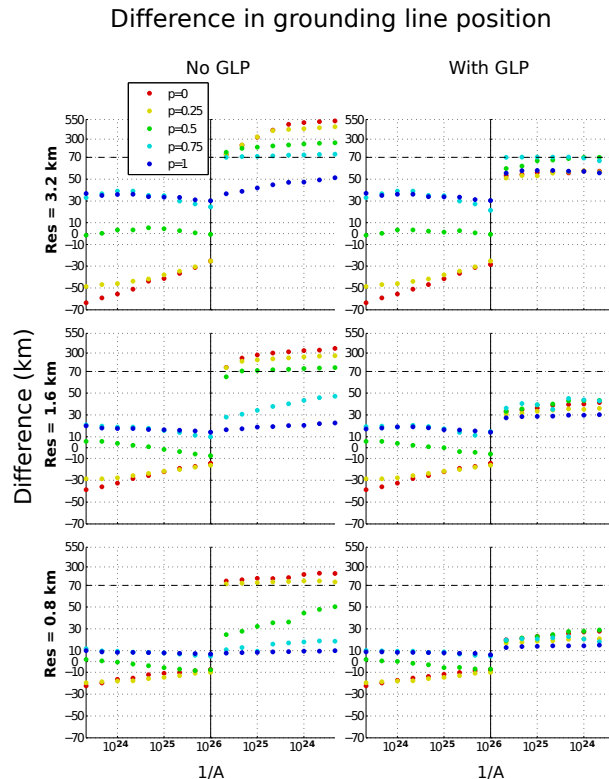


Fig. 6. The signed difference between the fixed-grid and benchmark grounding-line positions over a linear bed at 3.2 km (top row), 1.6 km (middle row) and 0.8 km (bottom row) resolution for simulations without GLP (left column) and with GLP (right column). Each column contains both advance (sub left column) and retreat (sub right column) experiments. Errors (absolute differences) are approximately inversely proportional to the resolution and decrease with increasing p , dramatically so without the GLP. The GLP reduces the most egregious errors during retreat (for small p).

Title Page

Abstract

Introduction

Conclusions

References

Tables

Figures

◀

▶

◀

▶

Back

Close

Full Screen / Esc

Printer-friendly Version

Interactive Discussion



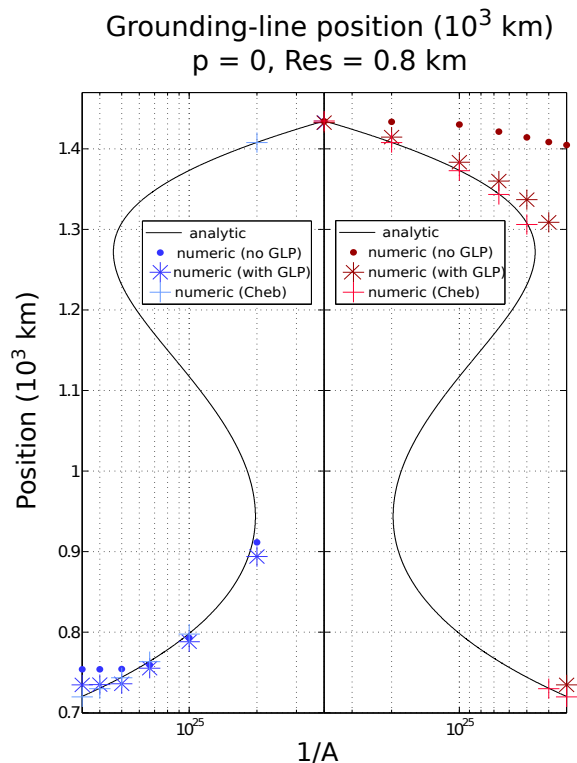


Fig. 7. As in Fig. 5 but with the polynomial bed shown in Fig. 2a. The boundary-layer solution closely agrees with Chebyshev results (maximum difference of 1.4 km). The fixed-grid results with the GLP also compare well with the benchmark (maximum difference of 31 km) except in the immediate vicinity of the unstable region. Without the GLP, the fixed-grid grounding line follows the boundary-layer solution reasonably well during advance (maximum error of 34 km) but not during retreat (maximum error of 110 km when both Chebyshev and fixed-grid solutions are on the same side of the unstable region, 690 km otherwise).

Parameterization of basal hydrology near grounding lines

G. R. Leguy et al.

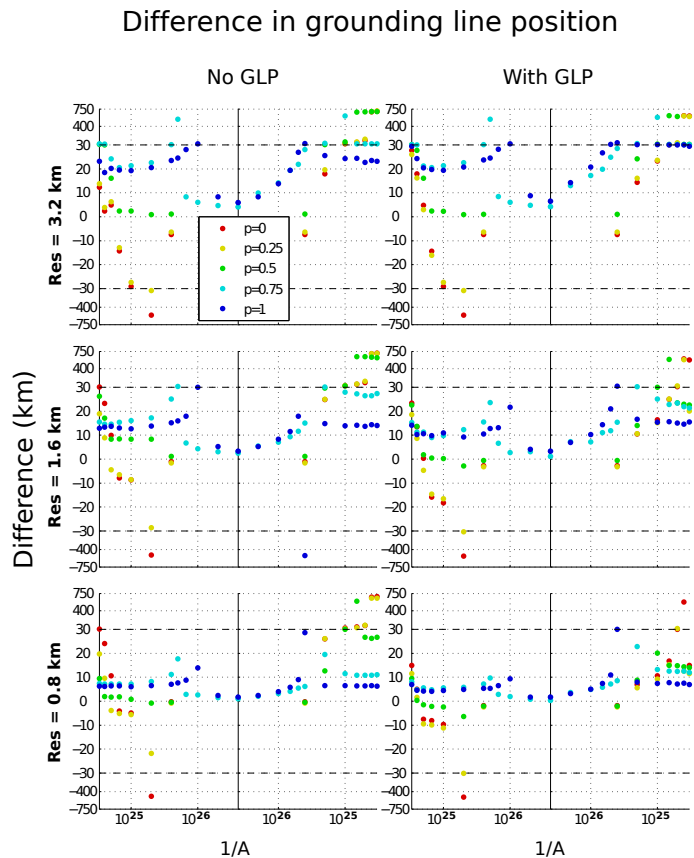


Fig. 8. The signed difference between the fixed-grid and benchmark grounding-line position as in Fig. 6 but with the polynomial bed. Errors (absolute differences) without the GLP are approximately inversely proportional to the resolution and decrease strongly with increasing p . With the GLP, the difference is inversely proportional to the resolution but does not decrease as dramatically with increasing p .

Parameterization of basal hydrology near grounding lines

G. R. Leguy et al.

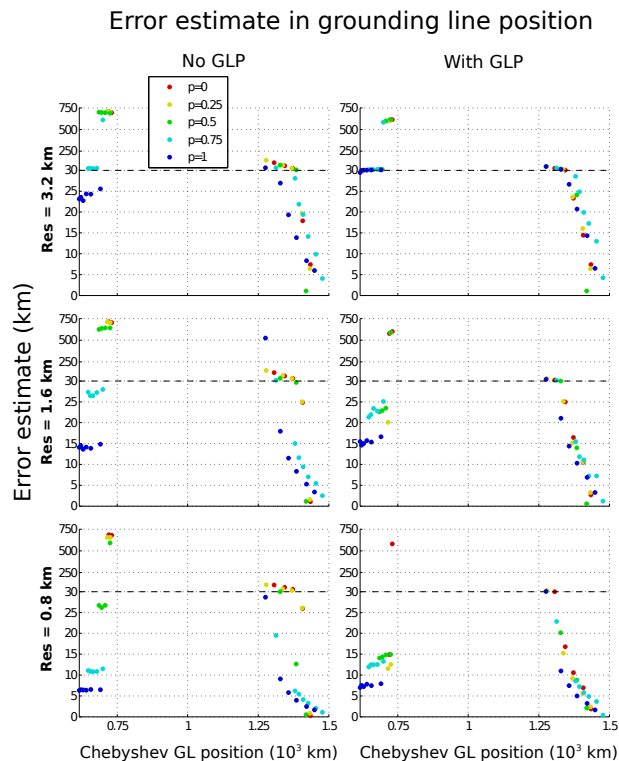


Fig. 9. As in Fig. 8, but showing only the retreat experiment with benchmark grounding-line position instead of A along the x -axis. The error in grounding-line position is consistently lower at a given grounding-line position when $p = 1$ than for smaller values of p . The figure shows that the grounding line approaches the unstable region (empty gap in each figure) more closely when $p = 1$ than for other values of p , perhaps explaining the anomalously large errors at these values of x_G .